

<https://doi.org/10.1038/s42003-025-08959-z>

Intercellular signaling and synaptic deconstruction uncovered by single-cell and spatial transcriptomics in an AD tauopathy model



Jeff X. Ji^{1,5}, Brian L. Giles^{1,5}, Surjyadipta Bhattacharjee^{1,5}, Marie-Audrey I. Kautzmann¹, Alasdair P. Masson¹, Sonia Do Carmo², A. Claudio Cuello^{2,3,4} & Nicolas G. Bazan¹ ✉

Alzheimer's disease (AD) is the leading cause of dementia in elderly individuals worldwide; however, all mechanisms leading to disease onset and progression are not well understood. Here, we report brain single-cell multiome and spatial transcriptomics in a transgenic rat model of human-like tauopathy. We have identified new markers of tau-driven AD pathology and provided single-cell evidence for genes implicated in AD. Our findings reveal how tau hyperphosphorylation and aging alter ligand-receptor communication, transcription factor regulatory networks, and specific cellular networks. Notably, we found intriguing changes in cell communication involving glutamatergic transmission and Netrin signaling as a tauopathy consequence. Overall, this study reinforces the concept that synaptic dysfunction is a critical early event in AD and highlights potential targets as potential therapeutic strategies.

Alzheimer's disease (AD) primarily affects the elderly population, leading to progressive cognitive decline and memory loss. It is the most common cause of dementia, accounting for 60–80% of cases worldwide^{1,2}. The hallmark pathology of AD includes extracellular accumulation of amyloid-beta (A β) plaques and the intracellular formation of neurofibrillary tangles (NFT) composed of hyperphosphorylated tau proteins. These aggregates disrupt neuronal function and trigger a cascade of disease-aggravating events, notably neuroinflammatory responses, which contribute to neuronal cell damage and death^{2,3}.

Understanding the mechanisms underlying AD is necessary for developing effective therapeutics. Animal models are valuable tools to study the cellular and molecular changes leading to AD^{4–6}. Rats offer advantages over other models, including larger brains and advanced behavioral aptitude that make them more suitable to study cognitive, biochemical, electrophysiological, and imaging-related features of tauopathies⁷. Of relevance to tau pathology, rats, like humans, display endogenous expression of all six tau isoforms⁸, and the C-terminal half of their tau protein, implicated in tau misfolding, is highly homologous to human tau⁹. These attributes make rat

models particularly suitable for studying the intricate processes involved in tauopathy and their implications for AD.

We utilize the AD rat model R955-hTau^{+/+}, which overexpresses the 2N4R isoform of human Tau protein with the FTDP-17T P301S mutation, to investigate the transcriptional and epigenetic landscapes of the hippocampus in rats affected by tau hyperphosphorylation and NFT aggregation. By applying single-nuclei RNA sequencing (snRNA-seq) and assay for transposase-accessible chromatin using sequencing (snATAC-seq), we have enabled high-resolution analysis of gene expression and chromatin accessibility at the single-cell level to define regulatory events that contribute to tau-induced neurodegeneration. We focused on early (10-month) and late (20-month) pathology of the rat Tau model to provide insights into changes during aging and with disease.

In the APP rat model of AD, the dysregulation of synaptic plasticity-related genes, such as *Grin1*, *Grin2b*, *Dlg4*, *Syn1*, and *Camk2b*, was reported¹⁰. Subsequently, a study of AD tauopathy in a rat model showed a decrease in the synaptic marker NMDAR1 and axonal marker NF-L;

¹Neuroscience Center of Excellence, School of Medicine, Louisiana State University Health New Orleans, New Orleans, LA, 70112, USA. ²Department of Pharmacology & Therapeutics, McGill University, Montreal, H3G1Y6, Canada. ³Integrated Program in Neuroscience, McGill University, Montreal, H3A 1A1, Canada. ⁴Department of Pharmacology, Oxford University, Oxford, OX13QT, UK. ⁵These authors contributed equally: Jeff X. Ji, Brian L. Giles, Surjyadipta Bhattacharjee. ✉e-mail: nbazan@lsuhsc.edu

however, a comprehensive study on the expression of synapse-associated genes is lacking¹¹. Cognitive decline is positively correlated with the number and extent of NFT formed by Tau, which is likely due to the loss of synapses during early stages of AD^{12,13}. In this context, we sought to explore consequences of tau toxicity in relation to synaptic dysregulation. Using gene enrichment analysis, we identified pathways related to the disruption of axon guidance and perturbation of synapse assembly at early stages of human-like tauopathy. This reinforces the concept of initial synaptic failure in the continuum of AD pathology.

Results

Hippocampal cell diversity in R955-hTau^{+/+}

To explore the hippocampus cellular landscape of a rat model of AD-like tauopathy, we performed paired snRNA-seq and snATAC-seq by 10X Genomics Single Cell Multiome ATAC + Gene Expression from the hippocampus of 10- and 20-month-old transgenic rat R955-hTau (hereafter designated as Tau) and age-matched wild-type littermates. We obtained 57 cell clusters that were manually annotated according to the ABC atlas cell type subclasses (Fig. 1a and Supplementary Figs. 1–2).

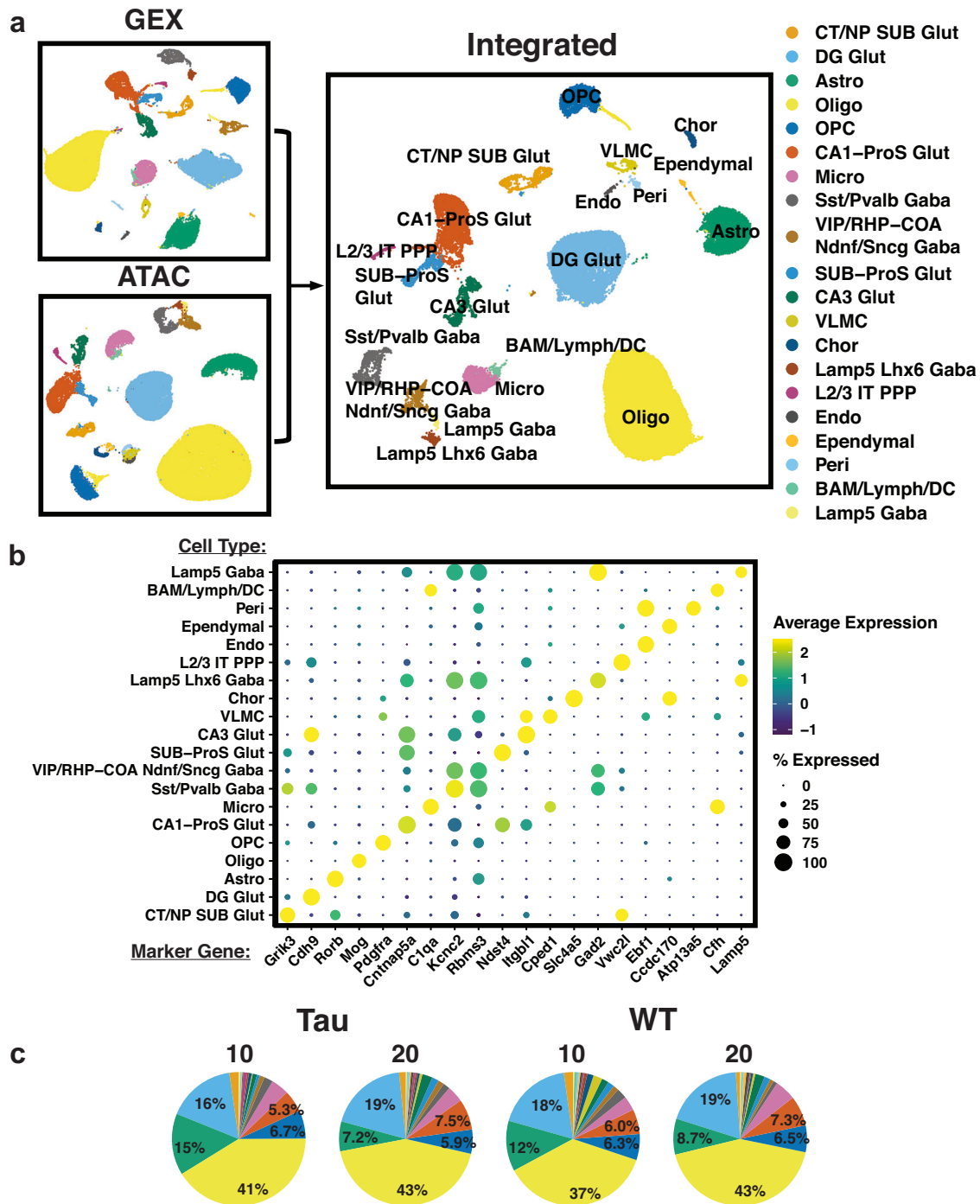


Fig. 1 | Hippocampal cell diversity in the R955-hTau transgenic rat model (Tau) and in WT. a Uniform manifold approximation and projection (UMAP) visualization of single-nucleus RNA-seq (GEX) and ATAC-seq (ATAC) integration map

depicting high-resolution clustering of single nuclei colored by cell type. **b** Dot Plot of cell-type-specific markers gene expression to identify each cluster in (a). **c** Cell proportions of each cluster by sample type.

The coloring scheme for each cell type in the weighted nearest neighbor (WNN) uniform manifold approximation and projection (UMAP) was preserved in subsequent figures. Cell classes with low total counts or outside the hippocampus were excluded from further analysis. A dot plot of the top marker gene for each of the cell types and a Feature plot of the top cell markers are shown in Fig. 1b and Supplementary Fig. 3. We did not observe significant differences in the proportion of cell types between Tau-10, Tau-20, WT-10, or WT-20 (Fig. 1c). Cell abundance ordered from highest to lowest are: oligodendrocytes (40.9%), dentate gyrus glutamatergic neurons (DG Glut) (18.3%), astrocytes (10.9%), CA1-Prosubiculum Glutamatergic neurons (CA1-ProS Glut) (6.5%), oligodendrocyte progenitor cell (OPC) (6.3%), Microglia (4.2%), somatostatin and parvalbumin GABAergic neurons (Sst/Pvalb Gaba) (1.9%), CA3 glutamatergic neurons (1.9%), corticothalamic near-project subiculum glutamatergic neurons (CT/NP SUB Glut) (1.8%), subiculum-prosubiculum Glutamatergic neurons (SUB-ProS Glut) (1.4%), neocortex neurons VIP/RHP-COA Ndnf/Sncg Gaba (1.2%), and cell types below 1% (vascular leptomeningeal cells, choroidal epithelial cells, endothelial cells, L2/3 IT PPP, Lamp5 Lhx6 Gaba, pericytes, ependymal cells, other immune cells, Lamp5 Gaba). Only cell types that constituted at least 1% of cells were considered for downstream differential expression and accessibility analysis.

Synapse signaling-associated gene signature alterations in hippocampal neuron subtypes in tauopathy

To assess cell-specific gene expressions in Tau at 10 and 20 months, we first performed pseudo-bulked differential gene expression for each of the main neuronal subtypes in the hippocampus. DG Glut in Tau displayed a greater number of differentially expressed genes (DEGs) at 10 months (61 genes, p -adjusted < 0.05) compared to 20 months (4 genes, p -adjusted < 0.05). There was a trend of greater changes at 10 months compared to 20 months for DE analysis of other cell types as well (Supplementary Dataset 1; contains tables of all differential expression comparisons). Comparing Tau-10 and WT-10 in DG Glut, top upregulated DEGs in Tau include *Chrm2*, *Col6a1*, *Efna5*, and *Ecel1*, while downregulated DEGs in Tau include *Pdzrn3*, *Grm8*, and *Scrn1*. The top DEGs at 20 months include *Chrm2* (up in Tau), *Cntnap5b* (down in Tau), and *Dennd2a* (down in Tau) (Fig. 2a). In CA1-ProS Glut, top upregulated DEGs include *Iqub*, *Epha10*, *Osbpl3*, and *Mapk4* at 10 months and *Lrrc36* at 20 months; top downregulated DEGs at 10 months include *Scrn1*, *Plekhh2*, *Grm8*, and *Ncald* at 20 months (Fig. 2a). In CA3 Glut, top upregulated DEGs in 10 months include *Mapk10*, *Atg16l1*, *Stxbp6*, and *Iqub*, and at 20 months *Stxbp6* and *Gabrg3*. Downregulated genes at 10 months old (mo) include *Ptgsd*, *Gpc3*, *Chst9*, and *Dpp10* (Fig. 2a). In addition to the pseudobulked DE analysis, the DEG analysis was also performed using a mixed-effects model that accounts for both subject-level and cell-level information and non-aggregated data without subject level information. The results are shown in Supplementary Dataset 2 and 3. Because pseudobulked DE analysis is the most statistically strict, resulting in the least number of statistically significant DEGs, thus minimizing the likelihood of false positives, it was used for pathway analysis and downstream analysis.

The barplots and visualization on reduced dimensional plots for select top DE genes are shown in Fig. 2d and Supplementary Fig. 4. Additional volcano plots for Tau versus WT comparisons in CT/NP SUB Glut and Sst/Pvalb Gaba neurons are in Supplementary Fig. 5. We observed genes related to synaptic components or that participate in synaptic development and organization. Thus, we selected gene-specific alterations in synapse-related genes to understand dysregulations at the pathway level. Gene enrichment analysis using the Gene Ontology Biological Process (GO BP) database compared the top DEG for Tau 10 vs. 20-mo. Pathway analysis using GO BP revealed disruptions in axon guidance and regulation of synapse assembly in Tau-10 and Tau-20 in DG Glut, Pros-CA1 Glut, and CA3 Glut neurons (Fig. 2b). We also observed alterations in pathways engaged in axon guidance, neuron projection guidance in DG glut, glutamatergic synaptic transmission and neurotransmitter transport in CA1-ProS Glut, modification of post-synaptic structure and dendrite development in CA3 Glut.

Additional GO MF and BP pathways for the above cell types are shown in Supplementary Figs. 6–8, including the top 15 significant pathways.

Given the prominence of the above processes to sustain synaptic integrity, mainly when challenged by an increasing burden of mutant tau, we examined the expression of genes that were altered in synapse-related pathways. For each neuronal cell type, we extracted the significant genes from each of the GO pathways shown in Fig. 2b and constructed a clustered heatmap of unique genes for each cell type. Notably, in DG Glut, there was decreased expression of adhesion coding genes such as *Cdh10*, *Nectin1*, and *Cntn4* in Tau-10 compared to WT-10. Cell adhesion molecules mediate cell-cell communications and interact with the ECM and are thus critical for synaptic development and for the establishment of neuronal networks. Interestingly, there was an upregulation of genes in the Semaphorin family (*Sema3c*, *Sema3e*), *Efna5*, and *Homer1* in Tau-10 (Fig. 2c). In the CA1-ProS, we observed a decrease in the expression of genes encoding glutamate receptors such as *Grid2*, *Grik4*, *Grm3*, and *Grm8* in Tau compared to WT. Additionally, there were alterations in the regulation of secreted factors such as *Ptn* (secreted heparin-binding growth factor), *Igf2* (insulin-like growth factor 2), and *Bdnf* (Brain-derived neurotrophic factor). Given the extent of gene alterations at 10 months between Tau vs. WT compared to 20 months, the early time point may offer a glimpse at a period of synaptic instability whereby the host of changes represents the simultaneous activation of neurodegenerative processes and repair pathways.

Glutamate receptor signaling is altered in early tauopathy

Having established that glutamate receptor encoding genes and glutamatergic synaptic organization pathways are disrupted in Tau, we sought to investigate whether neural communication is disrupted. We used NeuronChat¹⁴ to predict interneural communication networks through ligand-receptor interactions in specific neuronal and glial cells (Fig. 3a). From this workflow, a measure of communication probability was determined between each cell type for all interactions (Supplementary Fig. 9).

Non-peptide neurotransmitters are modeled based on the expression of synthesizing enzymes and vesicular transporters for the neurotransmitter. At 10 months, we observed a modest increase in the interaction strength and number of interactions in Tau (Fig. 3a). Furthermore, we found shifts in glutamate targets with decreased number of links for *Grm8* and *Grin3a* while there was an increase in the number of links for *Grm5*, *Gria2*, *Grik3*, and *Grm4* (Fig. 3c). At 20 months, there was a large increase in the number of inferred interactions with only a minor increase in interaction strength (Fig. 3b). We saw an increase in the number of inferred glutamate interactions with both ionotropic (*Gria4*, *Grin2a*, *Gria1*) and metabotropic receptors (*Grm7*, *Grm8*) (Fig. 3d) at late-stage Tau. Increased signaling through NMDA receptors such as *Grin2a*, *Grin2b*, *Grin1*, *Grin3a*, and *Grin2c* may lead to excitotoxicity in late-stage AD, which is characterized by neuronal loss and brain atrophy¹¹.

Given that the expression of glutamate receptors largely remains unchanged or is decreased in Tau-20 compared to WT-20, we reason that the increase in the number of links may be due to the upregulation of genes related to glutamate synthesis and reuptake. In both early and late tauopathy, altered glutamate signaling may lead to aberrant neuronal communication and contribute to the disruption of memory formation in the hippocampus.

Gene expression in glia engaged in sustaining synapses are altered by Tau burden and aging

The pivotal roles played by glial cells in the regulation of neuronal activity, response to injury, metabolic support, and the formation and maintenance of synapses lead us to perform pseudo-bulked differential gene expression comparing Tau and WT rats at 10 and 20 months for each of the main glial subtypes in the hippocampus, including astrocytes, microglia, oligodendrocytes, and OPCs. Top upregulated DEGs in astrocytes from Tau rats include *Retsat*, *Fbln2*, *Hdac4*, and *Cttna2* at 10 months, while top downregulated DEGs include *Fmn1*, *Pcdh11x*, *Ush2a*, and *Csmd3* at 10 months

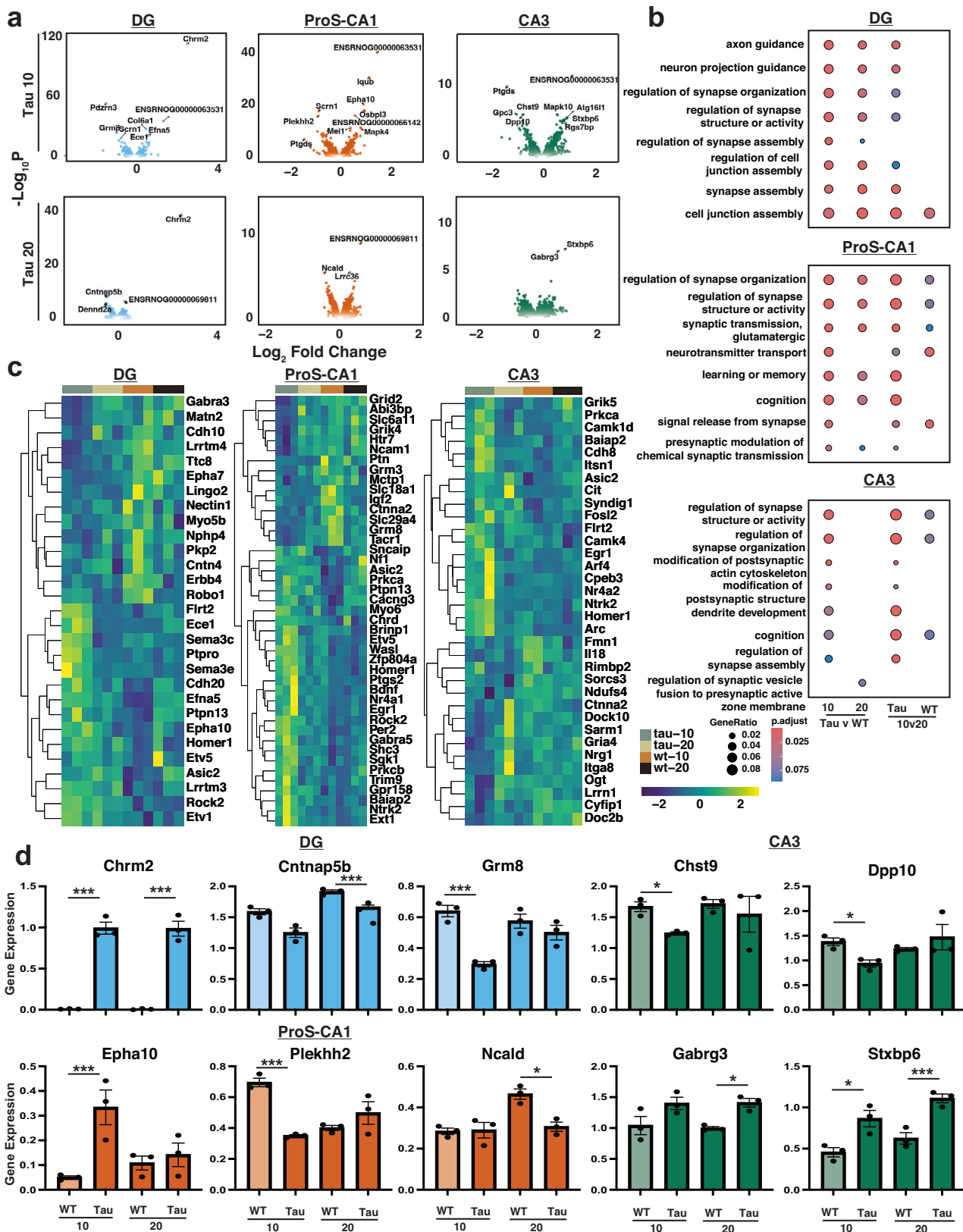


Fig. 2 | Genes related to synaptic modulation are altered in the Tau model. **a** Volcano plots showing DEG in 10-month-old and 20-month-old Tau rats and respective WT for the DG, ProS-CA1 and CA3 hippocampal regions. **b** Pathway enrichment analysis of genes related to synaptic modulation for each cell type. The

counts of enriched genes and adjusted P values are stated. **c** Heatmap of gene \log_2 fold changes (Log₂FC) composing the pathways in **(b)**. **d** Bar-plots showing the expression of representative genes from the volcano plots in **a** for DG, ProS-CA1, and CA3 neurons. Error bars are shown as mean \pm SEM.

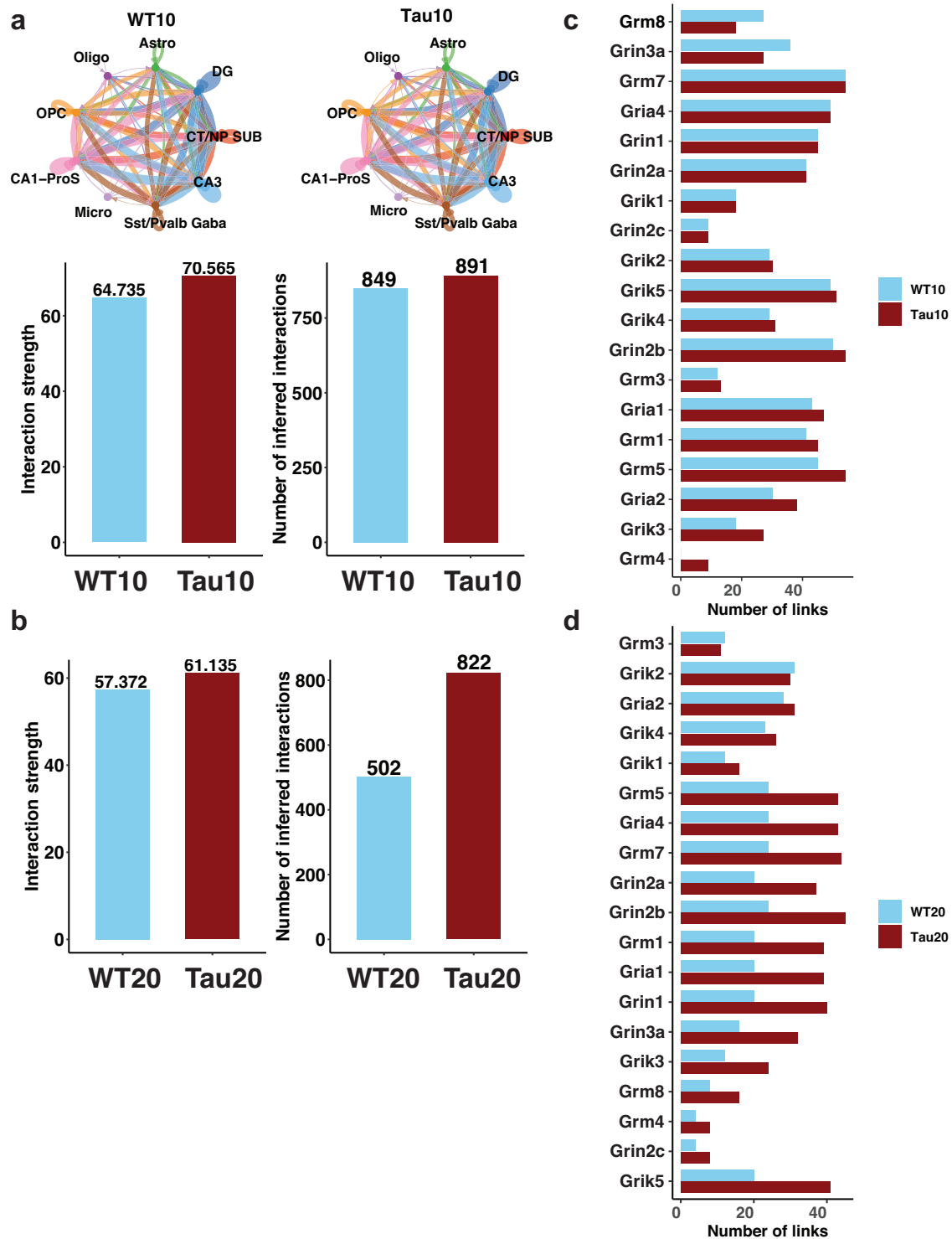


Fig. 3 | Glutamate signaling is altered in early and late Tau pathology stages in the AD-like Tau rat model. a Circle plot and bar-plot of interaction strength/number in 10-month-old Tau and WT rats. **b** Comparison of glutamate interactions between

20-month-old Tau and WT rats. **c** Bar chart comparing the number of links between 10-month-old Tau and WT rats. **d** Bar chart illustrating the number of links between 20-month-old Tau and WT rats.

and *Cntnap2* at 20 months. Microglial changes in Tau include upregulation of *Akr1d1*, *Fcrl2*, and *Sema3c* at 10 months and downregulation of *Lsamp*, *Ptprd*, *Csmd3*, and *Egf14* at 10 months. We did not observe significant changes at 20 months for microglia comparing Tau and WT. In oligodendrocytes, we observed an upregulation of *Skap2*, *Fut9*, and *Atp11b* in Tau-10 and downregulation of *Ctnnd2*, *Ltpr2*, *Robo2*, *Mccc2*, and *Scrn1* in Tau-10 as well as *Fam83d* in Tau-20 (Fig. 4a). Select genes with known links to AD development or synaptic modulation are shown in Fig. 4d.

Pathway analysis using GO BP revealed cell-specific changes in processes supporting synaptic maintenance. In astrocytes, there was enrichment in post-synapse organization, synaptic vesicle cycle, and signal release pathways from the synapse when comparing 10-month Tau and WT, 20-month Tau compared to 10-month Tau, and 20-month WT compared to 10-month WT. Pathways altered in microglia include cell-junction assembly, synapse pruning, and glial cell differentiation. Enriched pathways in oligodendrocytes include cell junction maintenance, protein

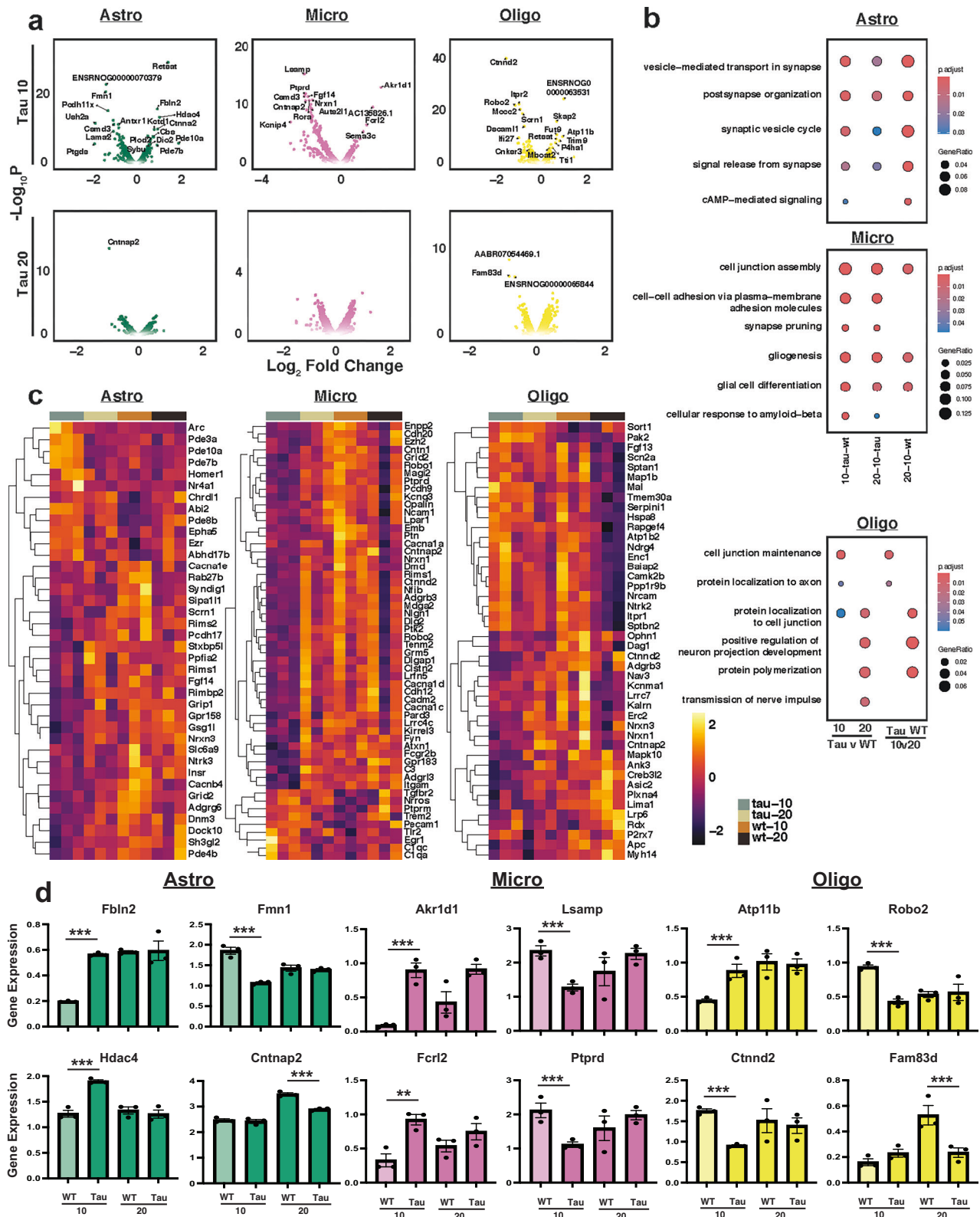


Fig. 4 | Expression of genes engaged in sustaining synaptic organization and function are altered in glial cells by Tau pathology burden and aging. **a** Volcano plots demonstrating DEG in astrocytes, microglia, and oligodendrocytes from 10-month and 20-month-old Tau rats, compared to respective WT. **b** Dot Plots showing

pathway enrichment analysis of genes related to synaptic modulation for each cell type. **c** Heatmap of \log_2 fold changes of genes representing the pathways in (b). **d** Bar plots depicting the expression of representative genes from the volcano plots in (a), for astrocytes, microglia, and oligodendrocytes. Error bars are shown as mean \pm SEM.

localization to the axon, positive regulation of neuron projection development, and transmission of nerve impulses. Additional pathway information for glial cells and volcano plots for OPCs are found in Supplementary Figs. 10–13 including the top 15 significant pathways. To study specific gene

dysregulations, we extracted significant genes from each of the GO pathways shown in Fig. 4b and constructed a clustered heatmap of unique genes for astrocytes, microglia, and oligodendrocytes (Fig. 4c). In astrocytes, we observed an upregulation of phosphodiesterase (PDE) genes (*Pde3a*,

Pde10a, *Pde7b*, *Pde8b*) in Tau-10. PDE participates in synaptic plasticity and homeostasis¹⁵, and inhibition of specific PDEs is a target of AD therapies¹⁶. We also observed a downregulation of astrocyte genes that regulate receptor function, such as *Gsg11* (regulation of AMPA receptor activity¹⁷), *Syndig1* (regulation of NMDA and AMPA receptor content¹⁸), and *Nrxn3* (regulation of aggregation of excitatory and inhibitory receptors). In Tau-10 microglia, there was an upregulation of genes (*Tgfb2*, *Nrros*, *Trem2*, and *C1qc*) that promote microglia anti-inflammatory phenotypes.

In oligodendrocytes from Tau rats, there was a downregulation of *Ctnnd2*, *Adgbr3*, *Cntnap2m*, *Nrxn1*, and *Nrxn3* gene expression involved in cell-contact and adhesion. Oligodendrocytes may be vulnerable to tauopathy-mediated axonal degeneration and, subsequently, myelin damage. Taken together, these results indicate that there are compensatory mechanisms in astrocytes, microglia, oligodendrocytes, and OPCs that act to sustain axonal and synaptic homeostasis.

Netrin signaling in OPC increases early in tauopathy

Thus, we have found gene expression changes in the hippocampus of Tau rats at 10 and 20 months, affecting both neurons and glial cells independently. Next, we investigated whether there are alterations in intercellular communication networks by advancing tauopathy. Since cell junction assembly and maintenance are altered in glia, we hypothesized that glial cell synaptic guidance is altered in advancing tauopathy. To explore the events contributing to neuronal death and cellular remodeling, we applied the computational tool CellChat to our Tauopathy model single-cell datasets. We calculated and plotted the total number of inferred interactions between Tau and WT for each age group. Using circle plots, we illustrated the number of intercellular interactions between the Tau and WT groups at 10- and 20-mo (Fig. 5a). Notably, the Tau 10-mo exhibited more interactions with stronger strengths between cells compared to aged-matched WT and Tau 20-mo compared to age-match control group (Fig. 5b). Moreover, to understand the signaling changes of groups, we compared the outgoing and incoming signal of each cell population in the early and late Tau model. We found that the signaling changes from all the cell populations were increased in Tau-10, while in Tau-20, there was notably a decrease in signaling from CT/NP SUB Glut, Oligodendrocytes and OPC (Fig. 5c). Due to their versatile nature of functions and their role in myelin formation, cellular signaling, phagocytic activity, and blood-brain barrier (BBB) formation and repair¹⁹, we assessed the types of signaling change in OPC of young and old animals. In the OPC of Tau-10, we observed a strengthening of the incoming signals from ADGRL, PTRP, and Netrin. On the other hand, there was a weakening of NCAM, CADM, and SEMA3 signals. At 20-mo, Netrin signaling in Tau was weakened (Fig. 5d). Moreover, interactions from the Netrin signaling pathway network driven by OPC (sender) showed that at 10-mo, the strength of interactions was stronger for DG Glut, CA3 Glut and Sst/Pvalb Gaba receiving (target) cells in Tau, while at 20-month, these interactions were stronger in WT vs. Tau (Fig. 5e). This is further confirmed with the information flow comparison of WT and Tau young and old animal, which recapitulated the sum of communication probabilities in OPC in the inferred network for Netrin signaling pathway.

We found that at 10 months, the Netrin signaling pathway was enriched in Tau but was less abundant at 20-mo (Fig. 5f). We then assessed the ligand-receptor pairs sensing from the OPC to receiving regions of Tau 10-mo. Netrin-1 ligand-receptor pairing was the most frequent in all cell types. Compared to WT, we found that Ntn1-Dcc signaling was increased from Tau OPC to Tau DG Glut, Astrocytes, OPC (autocrine effect), CA1-ProS Glut, Sst/Pvalb Gaba and CA3 Glut cells, while Ntn1-Unc5c pairing was higher from Tau OPC to Tau Oligodendrocytes and CA3 Glut (Fig. 5g). Western blot analysis of hippocampal Netrin-1 showed an increase in Tau-10 compared to WT-10 (Supplementary Fig. 14a). Previous studies have found that Netrin-1 co-localization with amyloid-beta plaques in the early stages of AD²⁰ and mutations in the Netrin-1 receptor Unc5c causes familial AD²¹. Taken together, our comparison revealed changes in Netrin signaling in early Tau. This highlights the role of Netrin-1 and its receptors as

enhanced signaling pairs from the OPC to the hippocampus, which could reflect a compensatory mechanism for the OPC to induce axonal growth and promote the repair of damaged synapses in tauopathy.

Identification of transcription factor impairments in early Tauopathy based on motif analysis

To determine how the epigenetic landscape is altered in Tau-10 and Tau-20, we first performed pseudo-bulked differential accessibility analysis for all the neurons and glial subtypes. Top differential accessible peaks (DAP) between Tau-10 vs. WT-10 and Tau-20 vs. WT-20 comparisons are found in Supplementary Figs. 15–18. After mapping peak regions to nearby or encompassing genes using the ClosestFeature function in Signac (see Online Methods). Tables for differential accessibility comparisons are in Supplementary Dataset 4. We noticed similar genes appearing in both the list of top differentially expressed and differentially accessible peaks when comparing Tau vs. WT at 10 and 20 mo. For example, in DG Glut, mRNA for *Chrm2* is significantly upregulated in Tau-10 compared to WT-10, while ATAC profiling shows increased accessibility at the promoter region and several sites along the coding region in Tau compared to WT (Supplementary Fig. 19). Additionally, there was a concentration of DAP in chromosome 4 for Tau-10 vs. WT-10. We highlighted cell-specific gene changes with corresponding changes in both mRNA and ATAC (Supplementary Figs. 19–20). Western blot analysis of the hippocampus revealed an increase in FBLN2 and CHRM2, as seen with the mRNA and ATAC at 10 months for astrocytes and DG Glut neurons, respectively (Supplementary Figs. 14 and 21).

We reasoned that DAP in Tau may be the result of altered transcription factor (TF) activity. Thus, we assessed at the single-cell level the gain or loss of accessibility from known TF motifs (JASPAR vertebrate database, see methods). The top gains and losses of motif accessibility/activity for glial cells (Fig. 6a, b) and neurons (Fig. 6c, d) between Tau-10 and WT-10 were plotted. Comparisons between Tau-20 and WT-20 are in Supplementary Fig. 22a, b. The motifs logos and ridge plot of chromvar z-scores of select TFs of interest in each cell type are depicted in Fig. 6b, d. In Tau-10 astrocytes, top motifs with increased accessibility include HOXB2, PDX1, EMX1, and GSX2 (Fig. 6a, b). GSX2 promotes injury-induced neurogenesis, and overexpression of *Gsx2* promotes astrocyte proliferation²². In Tau-10 microglia, top upregulated TF motifs include MEF2A-D, ZNF384, SPIC, and IRF1 (Fig. 6a, b). MEF2D is a stress-responsive TF that regulates interleukins and other inflammatory mediators in microglia²³. Overexpression of MEF2D in microglia reduces ischemic-reperfusion injury by decreasing microglia activation²⁴. In oligodendrocytes and OPCs, SOX15, FOSL1, and JUND TF showed greater activity in Tau-10 (Fig. 6a, b). Both SOX15 and FOSL1 families of TF are involved in the regulation of stem-cell programming^{25,26}. Overall, analysis of TF in glial cells reinforces their early role in initiating repair in response to accumulating misfolded tau by activating TF that counteracts inflammation and neurodegeneration.

Next, we examined top TF with increased activity in Tau-10 neurons. In Tau-10 DG Glut, the top TFs include DBP, HLF, TEF, and NFIL3. DBP, HLF, and TEF are members of the PAR bZIP family of TFs that are transcriptionally regulated by circadian oscillations. Overexpression of DBP in hippocampal neurons leads to impaired learning, increased seizure frequency, and ERK signaling²⁷. In CA3 Glut, ATF4 is upregulated in Tau-10. Interestingly, knockdown of ATF4 impairs long-term potentiation, reduces dendritic spine density, and increases synaptic excitability by reducing GABA receptor trafficking^{28–30}. We also found increased activity of TFs like POU3F1 and GABPA that regulate neural stem cell development^{31,32} in CA1-ProS Glut and CT/NP SUB Glut cells from Tau-10. The knockdown of *Pou3f* reduces adult hippocampal neurogenesis³³. TF highlighted in Fig. b, d, at 20-mo is shown in Supplementary Fig. 22c, d. In summary, our snATAC analysis provided complementary evidence of epigenetic dysregulation of DEG identified earlier, revealed patterns of altered chromatin accessibility across the genome in Tau, and identified putative TFs that are active in remodeling of specific neurons and glial subtypes in early tauopathy.

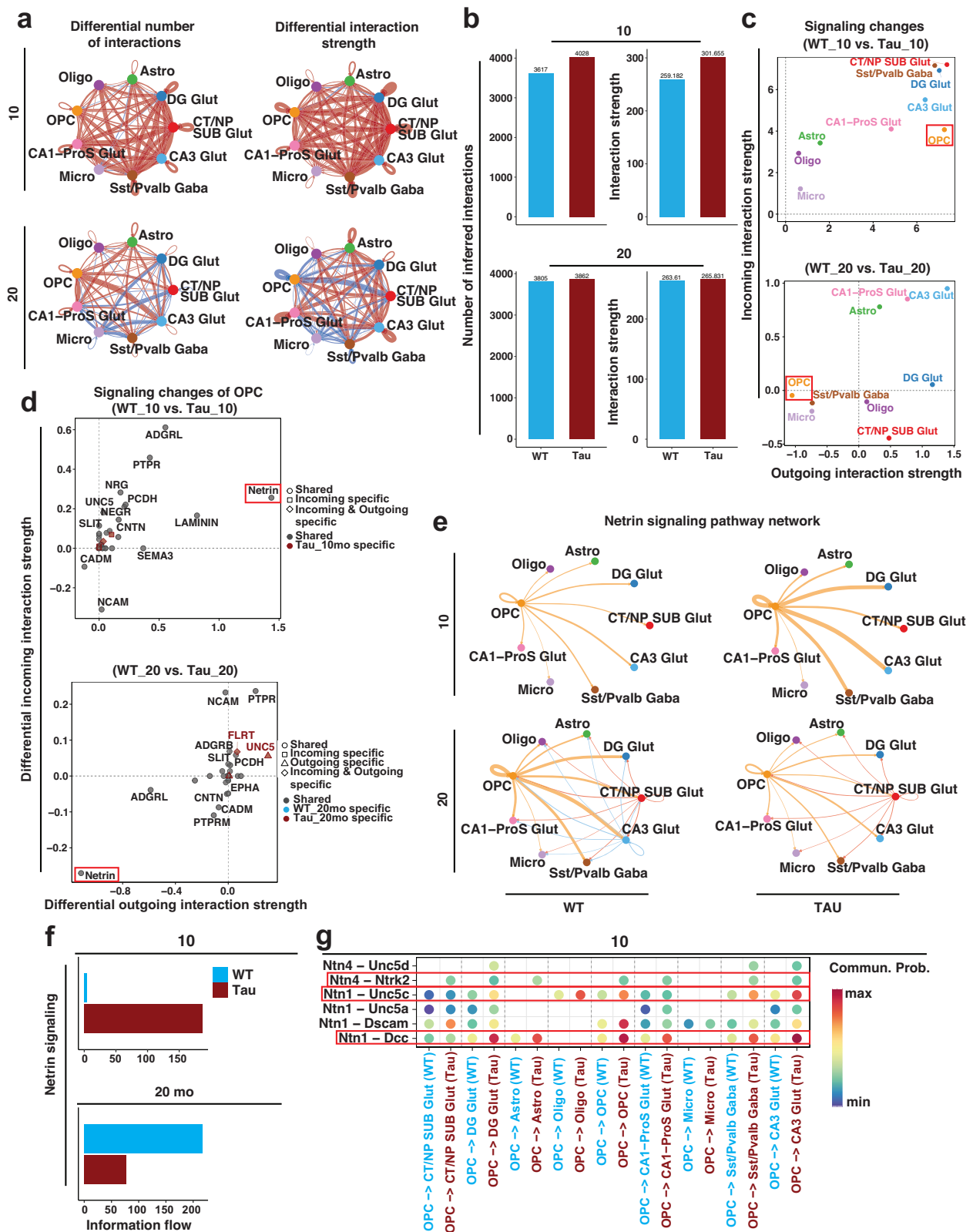


Fig. 5 | Netrin signaling alterations in OPC increases early in the Tau AD model. **a** Circle plots showing differential number of interactions and their strengths in 10- and 20-month-old Tau and WT rats. **b** Bar plots showing greater interaction number and strength in 10-month Tau rats. **c** Interaction strength in different cell types.

d OPC-specific signaling. **e** Netrin outgoing plots in Tau and WT rats. **f** Netrin signaling interactions at different ages. **g** Comparison of the significant ligand-receptor pairs between Tau and WT 10-month-old OPC.

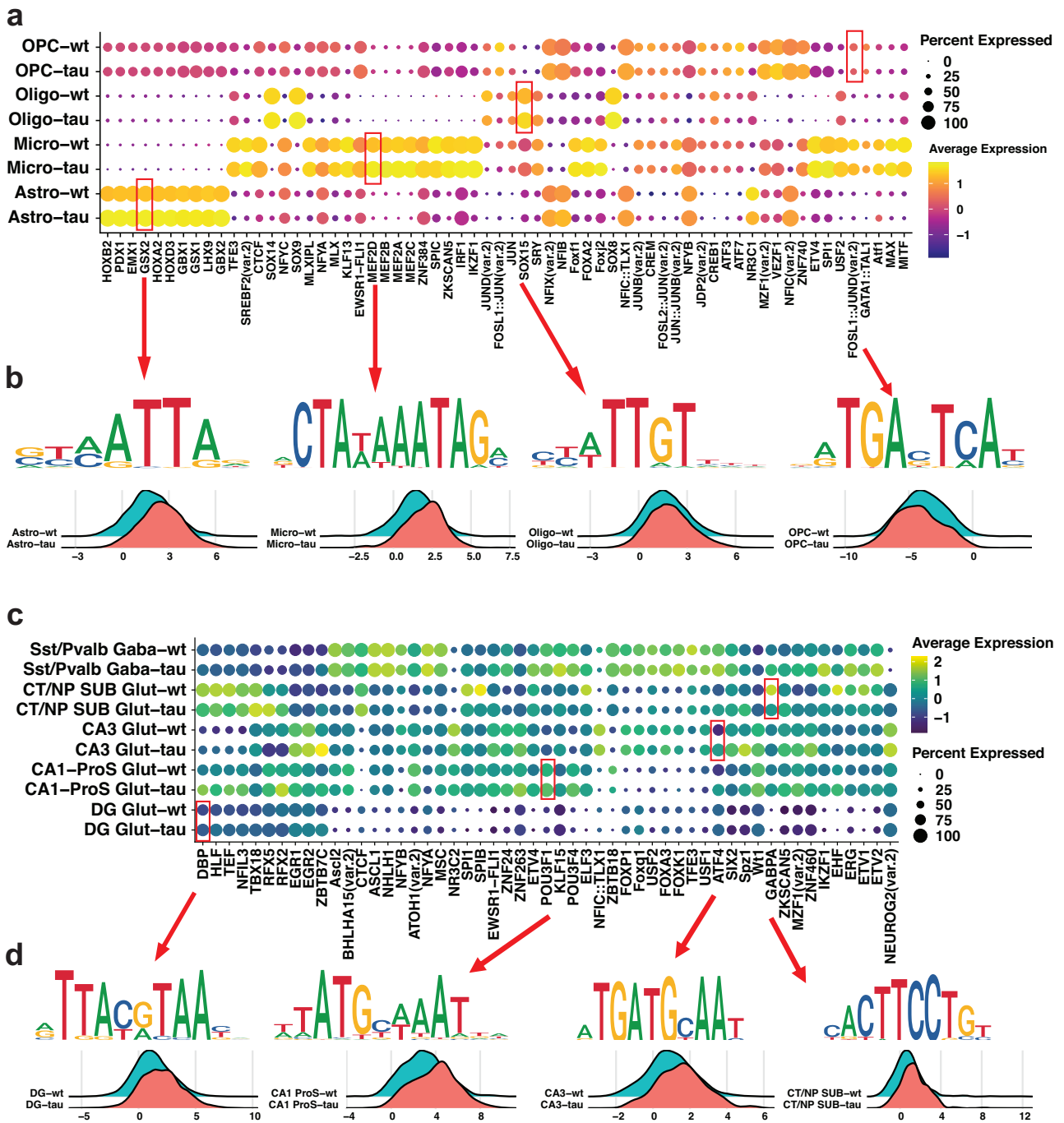


Fig. 6 | Identification of putative differences in cell-specific transcription factors between Tau and WT rats at 10 months of age. **a** Enrichment of the indicated TF motifs in astrocytes, microglia, oligodendrocytes and OPC. The size of each point represents the percentage of cells expressing this motif and the color of each point represents the motif enrichment P -value ($-\log_{10} P$ -value). **b** Transcription factor

binding site (TFBS) motifs for selected TF in each cell type are shown and associated ridge plots showing distributions of the Z-score of motif deviation scores in Tau and control rats. **c** TF motifs enrichment in DG Glut, CA1-ProS Glut, CA3 Glut, CT/NP SUB Glut, Sst/Pvalb Gaba neurons. **d** TFBS motifs of selected TF for specific cell types.

Longitudinal analysis of age-related gene changes in advancing tauopathy

We performed a non-aggregated DE analysis of WT and Tau animals at 10-mo and 20-mo to characterize the common effects of aging and unique changes due to the tauopathy. For each of the major cell types, the top DEGs that are specific to Tau or WT for each of the major cell types are shown in Supplementary Fig. 23. An interesting trend we observed is that there was a greater number of differentially expressed genes in the aged WT comparison over aged Tau, in most cell types with the exception of microglia. In

oligodendrocytes, there were 1037 DEGs in WT 20-mo to 10-mo compared to 249 in Tau. In WT oligodendrocytes, top aging DEGs include: *FAM135b*, *Skap2*, *Itrp2*, and *Robo2*. In Tau oligodendrocytes, top aging DEGs include: *Myof*, *Nrxn3*, *Mboat2*, and *Svep1*. In DG Glut, there were 751 DEGs in WT 20-mo to 10-mo compared to 444 in Tau. In DG Glut, top aging DEGs in WT include: *Mei1*, *Slc44a5*, *Pdzrn3*, and *Scrn1*. In Tau DG Glut, the top aging DEGs included: *Grm8*, *Col18a1*, *Fstl5*, and *Flrt2*. The full list of DEGs are available in Supplementary Dataset 5. In DG Glut neurons, we also applied a pseudotime analysis to characterize transition states between

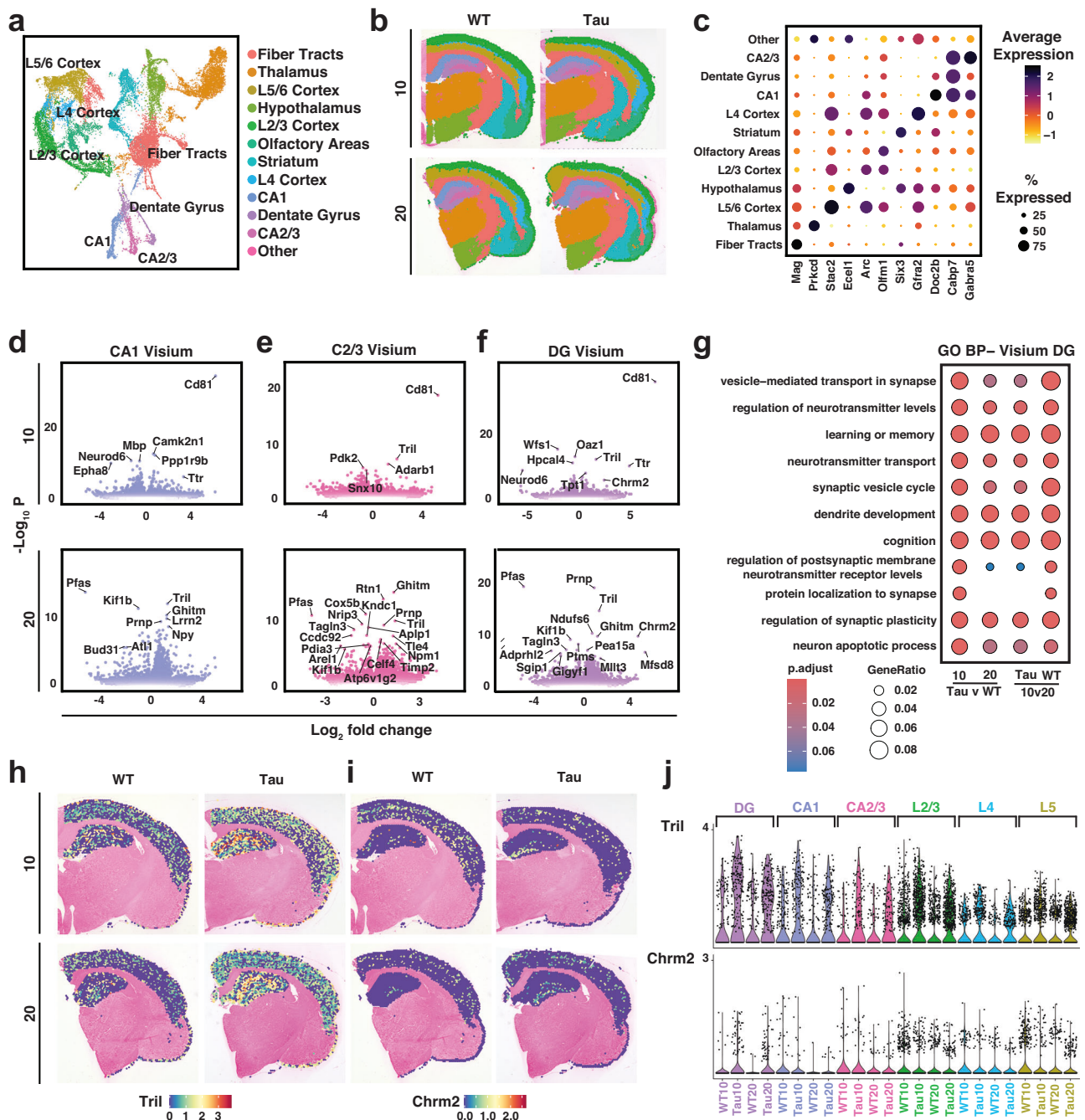


Fig. 7 | Spatial transcriptomics reveals modulation of neurotrophic signaling and synaptic changes in the Tau AD-like model. **a** UMAP derived from the spatial map. Cell types identified by marker genes. **b** Spatial maps of cell types in coronal rat brain sections. Cells are colored by their subclass identities. **c** Dot plot showing the expression of cell-specific markers for brain regions. **d–f** Volcano plot depicting differential abundance analysis of gene expression in 10 and 20-month Tau vs. WT rats for the CA1, CA2 + CA3 and DG hippocampal regions. The log₂ fold changes

are plotted on the X-axis. P-values (–log₁₀ P-value) are plotted on the Y-axis. **g** Gene Ontology Biological Processes enrichment analysis reveals the pathways that are up- and down-regulated in DG. **h** Spot plots of 10-month (upper) and 20-month (lower) coronal sections from Tau and WT rats depicting log(transformed normalized expression) (log(counts)) of *Tril* and (i) *Chrm2*. **j** Violin plots showing the expression of *Tril* and *Chrm2* per region and age.

young and aged cells in WT and Tau (Supplementary Fig. 24). We identified the origin as the cluster with the highest WT-10-month cells, which split into two trajectories. Trajectory 1 contains a higher proportion of cells from 20-mo Tau and WT, and trajectory 2 contains a higher proportion of cells from Tau 10-mo. Markers projected along trajectory 1 that corresponded to aging included *Sorcs3*, *Cdh10*, *Nrg1*, and *Arhgap6*. Trajectory 2 was most specific for Tau-10 months and was marked by *Col11a1*, *Adamts17*, and *Tspan18*.

Spatially informed subpopulations uncover cellular diversity in Tauopathy model

The spatial organization of cells enacts function and pathology in AD. To gain a deeper understanding of the cellular and molecular mechanisms underlying tauopathy, we analyze and map gene expressions within their spatial context. To this end, we performed spatial transcriptomics (10X Visium) of the brains of Tau and WT, young and old animals. After normalization of the data, we used a clustering-based approach and identified a

total of 22 clusters that were then manually annotated to the corresponding anatomical structures based on top marker genes for each cluster and its spatial location (Fig. 7a, b). Our data showed consistent capture of the same regions between Tau and WT (Fig. 7b). Top marker genes for each spatial region are shown in Fig. 7c, where known marker genes, such as *Cabp7*, are found in the DG, CA1 and CA3, *Mag* in the fiber track and *Stac2* in the L4, L5/6 cortex. We focused our DEG analysis on regions of the hippocampus, cortex, and fiber tracts. DEG comparisons of hippocampal regions between Tau-10 and WT-10 are shown in Fig. 7d–f. Other DEG comparisons are in Supplementary Fig. 25. We found the upregulation of *Cd81*, which is involved in neuronal migration and axon guidance³⁴, in Tau-10 in CA1, CA2/3, and DG regions. In DG and CA3 regions, we found downregulation of *Neurod6* in Tau-10 (Fig. 7d, f), which is a downregulated neuronal marker for AD³⁵. Pathways analysis in DG (Fig. 7g) and other brain regions recapitulated multiome findings of disruptions in synaptic function, including regulation of neurotransmitter levels, regulation of synaptic plasticity, protein localization to synapses in Tau compared to WT or between younger and older animals. In concordance with our multiome data, *Chrm2* is upregulated in the DG of Tau-10 and Tau-20 compared to WT (Fig. 7f, i, j). Additionally, we highlight the upregulation of *Tril* in the hippocampus and cortex in Tau-10 and Tau-20 (Fig. 7f, i, j). *Tril* is a TLR4-interacting protein that is linked to increasing neurofibrillary tangles in human AD³⁶.

Decreased BDNF signaling in the DG of early tauopathy

We next examined if tauopathy disrupted cell-cell communication using spatially resolved transcriptomics data, which identified secreted signaling interactions between different brain regions (Fig. 8a). We found an overall increase in total interaction strength in Tau-10 and Tau-20 compared to WT (Fig. 8b). Despite the increase in total interaction strength in Tau, there was a reduction in neurotrophic signaling in Tau-10 and Tau-20 originating from the dentate gyrus to hippocampal regions such as CA1, DG, and CA2/3 from *Ntf3-Ntrk2* and *Bdnf-Ntrk2* signaling (Fig. 8d), which could be explained by the downregulation of *Bdnf* in Tau-10 (Fig. 8c). Interestingly, the *Bdnf-Ntrk2* signaling originating from cortical layer L2/3 to L4 and L5/6 increased in Tau-10 and Tau-20 (Fig. 8d, e). In both early and late tauopathy, we observed a shift in the neurotrophic signaling from predominantly in DG in WT to L2/3 Cortex in Tau (Fig. 8f). Analysis of NT signaling using multiome data did not reveal differences (Supplementary Fig. 26). Depletion of BDNF in the hippocampus may result in impaired synaptic maintenance and is associated with A β accumulation, tau hyperphosphorylation, and inflammation in AD³⁷.

Discussion

The main correlate of cognition decline in AD is the accumulation of tau pathology, which is linked to local neurodegeneration. The mechanisms underlying neurodegeneration in AD are complex and involve intricate interactions between neurons, glia, and the extracellular environment. Thus, identifying disease mechanisms in AD will benefit from a cell-specific understanding of the gene networks and epigenetic changes that mediate the adaptive and maladaptive responses, ultimately leading to brain atrophy. Our multiome and spatial study of the brain in a rat model of human-like tauopathy revealed novel transcriptomic, epigenetic, and cell-cell communication disruptions in early and late AD-like tauopathy. We noted differences in genes related to synaptic organization and transmission, mainly in early tauopathy in distinct neurons, and in glial populations, genes that were associated with altered glutamatergic signaling in both early and late AD. In early AD, we identified TFs implicated in repair and regenerative response after neural injury and identified increased Netrin signaling in early tauopathy. Additionally, we identified spatially resolved gene expression changes in distinct anatomical regions of the brain and a reduction in neurotrophic signaling, specifically *Bdnf* and *Ntf3*, in the hippocampus in early and late AD.

It is well known that synaptic degeneration correlates with memory loss and cognitive decline in AD³⁸. However, the cell-specific changes that cause synaptic dysfunction due to abnormal tau phosphorylation and

aggregation are still under active investigation. There are currently only a few single-cell/nuclei studies of neuronal-driven expression of mutant tau that aim to establish a model of AD. In a THY-Tau22 mouse model, Ali and colleagues³⁹ found differences in pathways engaged in synapse organization, cell junction disassembly, and gliogenesis in male and female THY-Tau22 animals. Our pathway analysis using GO revealed alterations of genes that regulate synapse organization and assembly, as well as glutamatergic synaptic transmission in hippocampal neuron subtypes due to tauopathy. We observed reduced gene expression of glutamate receptor *Grm8* in DG/CA1-ProS Glut neurons in Tau at 10 months, decreased *Dpp10* on CA3 Glut neurons in Tau at 10 months, and increased *Epha10* in CA1-ProS Glut neurons in Tau at 10 months. GRM8 is a metabotropic glutamate receptor downregulated in neurons from multiple sclerosis patients⁴⁰ and its knockdown increased neuronal sensitivity to glutamate excitotoxicity⁴⁰. The reduction of *Grm8* in neurons may represent a loss of neuroprotective mechanism to counteract excitotoxicity in tauopathy and suggest a disruption in the production of glutamate receptors. However, the decrease in *Grm8* was not present in neurons in Tau at 20 months. NeuronChat analysis provided evidence of increased glutamate signaling in early and late tauopathy and greater glutamatergic signaling through receptors such as *Gria1/4/5*, *Grin2a/b/c*, and other glutamate receptors. In a Tg4510 mouse model of tauopathy, increasing neuron excitability with age takes place⁴¹ and increased excitatory activity despite neuron atrophy and a reduction in dendritic spine density⁴².

The changes in synaptic genes starting at Tau 10 months correlate well with previous evidence of synaptic dysfunction in this model. R955-hTau +/+ rats exhibit progressive cognitive impairments, beginning with social interaction deficits at 9 months, as demonstrated in the 3-chamber test. These impairments advance to deficits in novel object recognition and location and in Morris water maze tasks at 14 months, which become more pronounced by 20 months¹¹. Additionally, we previously reported that in R955-hTau +/+ rats, synaptic alterations occur sequentially. First, there is a decrease in NMDAR1 (*GluN1*) protein levels at 9 months, followed by a reduction in synaptophysin immunofluorescence (IF) at 14 months, and ultimately, a loss of MAP2 IF and NF-L at 20 months of age¹¹. These findings are consistent with the early loss of synaptophysin observed in Alzheimer's disease, followed by more pronounced axodendritic degeneration in later stages of the disease. In R955-hTau +/- rats, a milder version of the transgenic model that does not exhibit significant neuronal loss or NFT-like structures. We observed that 20-month-old R955-hTau +/- rats, which display a phenotype similar to that of 10-month-old R955-hTau +/+ rats, exhibit impaired responses to high-frequency stimulation (HFS) for inducing long-term potentiation (LTP) in the CA1 region of the hippocampus during acute brain slice electrophysiology⁴³.

We observed a consistent upregulation of *Chrm2* in DG Glut neurons in both early and late tauopathy. *Chrm2* encodes a cholinergic muscarinic receptor involved in the modulation of neurotransmitter release and other synaptic functions⁴⁴. CHRM2 activation impairs the release of acetylcholine in brain regions involved in learning and memory⁴⁴, and selective inhibition of the M2 receptor improved cognition in rats⁴⁵. Additionally, CHRM2 is increased in the frontal and temporal cortex of patients with AD and psychotic symptoms⁴⁶. Our data showed an upregulation of *Chrm2* gene expression in both snRNA and spatial transcriptomics, as well as increased chromatin accessibility at the gene promoter at 10 and 20 months in DG neurons in Tau with snATAC. GWAS SNP studies have consistently linked CHRM2 with cognitive processing and intelligence⁴⁷. Whether the upregulation of *Chrm2* acts to restore or disrupt homeostasis in the DG is unknown. Recent clinical trials have shown that positive allosteric modulators for CHRM1/4 have a role in the treatment of schizophrenia^{48–50}. A novel CHRM2 function was recently uncovered, showing that the C-terminus domain of CHRM2 is selectively localized to the mitochondria of stressed cells to reduce oxidative stress⁵¹. In this way, *Chrm2* upregulation may be a protective mechanism to counteract mitochondrial damage and oxidative stress due to the accumulation of hyperphosphorylated tau⁵². Our trajectory analysis of DG Glut neurons from 10 and 20 months revealed a

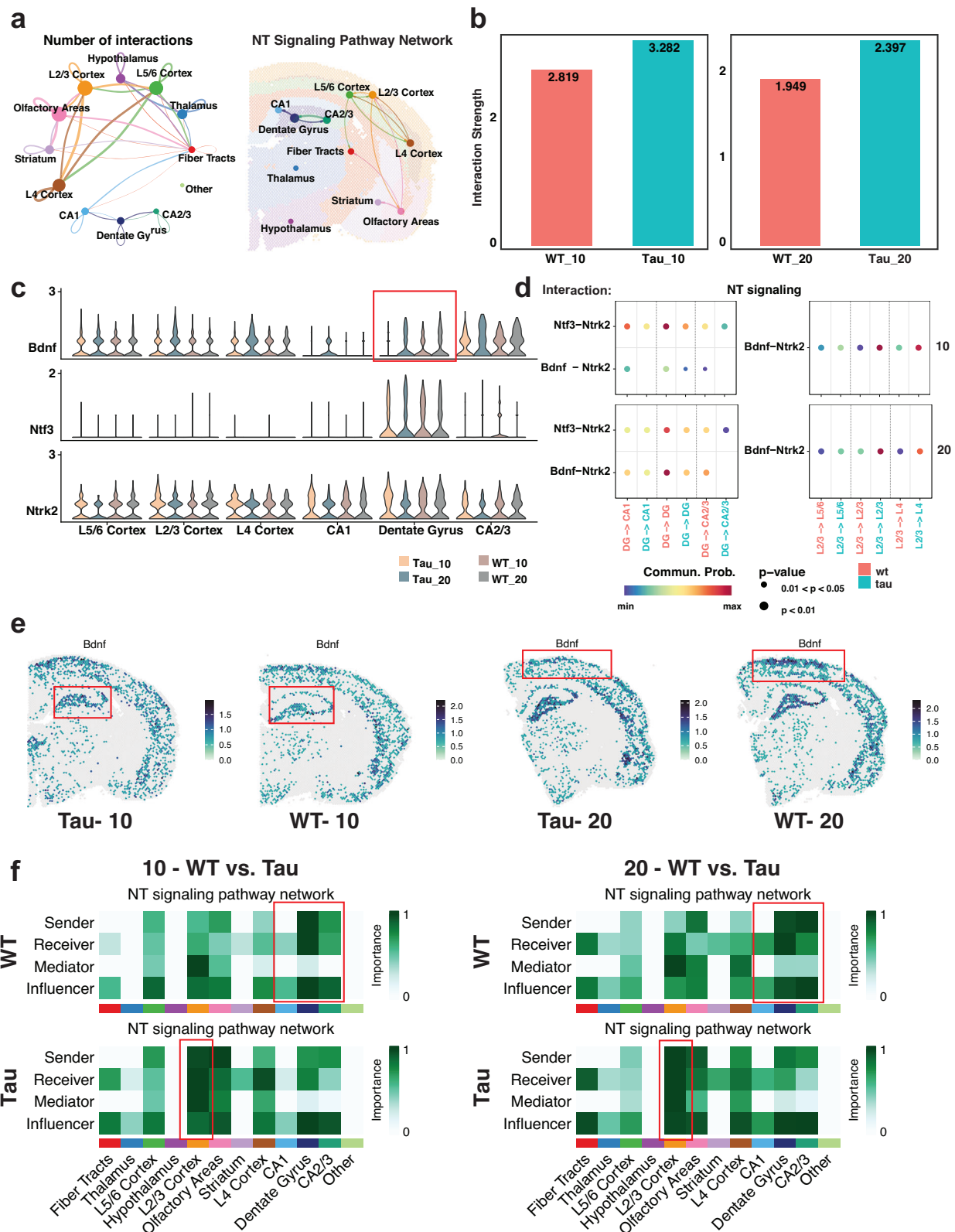


Fig. 8 | Spatial transcriptomic and CellChat analysis demonstrate modulation of neurotrophic signaling in Tau hippocampus. a Circle plot (left) showing the number and the degree of interactions between brain regions in WT 10-month, and visualization outputs (right) for NT signaling analysis in the spatial context. **b** Interaction strength depicted by bar plot in Tau and WT, 10- and 20-month. **c** Violin plots displaying the expression level of *Bdnf*, *Ntf3*, and *Ntrk2* in different

brain regions of Tau and WT, 10- and 20-month. **d** Dot plot showing the degree of interactions focused on NT signaling, between regions. **e** Feature plot showing the expression distribution of *Bdnf* in WT and Tau 10-month and 20-month. **f** Heatmap showing the relative importance of each brain region based on the computed four network centrality measures of NT signaling network in Tau vs. WT at 10- and 20-month.

trajectory that corresponded to aging and another specific for Tau 10-mo, which corresponds to early tauopathy. *Nrg1* was a marker found in the aging trajectory, and serum levels of *NRG1* have been shown to be elevated in AD patients with mild cognitive impairment and dementia⁵³. *Adamts17* was one of the markers defining the trajectory for early tauopathy. *ADAMTS17*, a metalloproteinase with largely unknown function in the brain, has been shown to interact with *Fibulin-2* in chondrocytes⁵⁴.

Glia are disrupted by the abnormal accumulation of aggregated tau. Astrocytes participate in the recycling of neurotransmitters, as the glutamate-glutamine cycle⁵⁵, while microglia participate in pro- and anti-inflammatory signaling and are crucial for pruning of synapses⁵⁶. Aside from myelination, oligodendrocytes and OPCs are involved in synapse formation and maturation and metabolic processes^{57,58}. Astrocytes, microglia, oligodendrocytes, and OPCs are key in the development of neurodegeneration in AD. GO pathway analysis revealed enrichment of pathways that include vesicle-mediated transport in the synapse, post-synapse organization, and cAMP-mediated signaling in astrocytes; cell junction assembly, synapse pruning, and cellular response to amyloid-beta in microglia; cell junction maintenance, positive regulation of neuron projection development, and transmission of nerve impulses in oligodendrocytes. These pathways highlight changes in interactions between glial cells and neurons at the synapse. We observed an increase in *Fbln2* in astrocytes and oligodendrocytes in early tauopathy as well as aging. *FBLN2* is released into the extracellular matrix, where it inhibits OPC maturation by activating Notch signaling⁵⁹. Previous studies have highlighted the upregulation of *FBLN2* in the spinal cord in experimental autoimmune encephalitis (EAE) and in the brain from patients with multiple sclerosis⁵⁹, as well as increased *FBLN2* protein in the CSF after TBI⁶⁰ and AD⁶¹. In the EAE model, astrocyte-specific depletion of *Fbln2* using CRISPR/Cas9 increased oligodendrogenesis and improved functional outcomes by improving remyelination of the spinal cord⁶¹. Interestingly, astrocyte secretion of small extracellular vesicles containing *FBLN2* increased spine and synapse formation through TGF-beta signaling⁶². Following traumatic brain injury in a mouse model, *Fbln2* was elevated in the injury site and co-localized with GFAP-expressing astrocytes⁶². While the role of *FBLN2* in AD is still unknown, *fibulin-1* was elevated in serum exosomes from patients with mild cognitive impairment, a prodrome for AD⁶³. *FBLN2* upregulation at Tau-10mo in astrocytes highlights the complex interplay between processes that promote and oppose synaptogenesis and myelin formation. It is possible that selective signaling to neurons but not to OPCs using small extracellular vesicles containing synaptogenic cargo as a therapeutic strategy to promote synapse regeneration without compromising oligodendrocyte maturation.

Using CellChat, we found an overall increase in the number and strength of cell-cell communications in the R955-tau animals at 10 months compared to wild-type. OPCs showed opposing patterns in total signaling changes in early and late tauopathy, with increased outgoing interaction strength at 10 months but decreased outgoing interaction strength at 20 months in tau compared to wild-type animals. More specifically, Netrin signaling stood out in OPCs as the most elevated pathway in tau at 10 months compared to WT, but showed the reverse trend at 20 months. Netrin outgoing signals originated predominantly in OPCs that strongly signaled to neurons over oligodendrocytes, astrocytes, and microglia. There were greater interactions between *Ntn4-Ntrk2*, *Ntn1-Unc5c*, and *Ntn1-Dcc* in tau animals compared to WT at 10 months. Netrin signaling is known to be involved in the growth cone and axonal guidance^{64,65}. Netrin is intimately involved in synaptogenesis and plasticity by recruiting post-synaptic proteins, such as PSD-95 and GluA1 AMPA receptors, and the presynaptic protein synaptophysin⁶⁶. Applications of Netrin-1 alone induced LTP at Schaffer collateral-CA1 synapses⁶⁷ and may increase presynaptic signaling through the Netrin receptor *DCC*⁶⁸. Previous animal studies have found that Netrin-1 is neuroprotective against the loss of memory, corrected late-phase LTP impairments⁶⁹, and suppressed A β 42 production⁷⁰ in mouse models of AD. Furthermore, Netrin-1 was significantly decreased in the serum from AD patients⁷¹ and decreased in the serum and CSF from the A β 42 model of

AD⁷². Our findings suggest that Netrin signaling initially rises as a compensatory response to toxic tau accumulation and impaired axonal transport, aiding synaptogenesis in the early stages of tau-mediated AD. However, the impact of tauopathy on Netrin signaling remains largely unexplored. However, the Netrin-1 receptor *DCC* interaction with *MAPT* inhibited axonal outgrowth⁷³. Failure of Netrin signaling is seen in our data at 20 months and in aging human brains and brains of Parkinson's disease patients²⁰.

We observed fewer DEGs between Tau and WT at 20 months for glial cell subtypes compared to 10 months. A similar observation was made in a *Drosophila* model of AD pathology expressing pan-neuronal human tau, where 70% of the tau-induced DEGs were also altered during normal aging⁷⁴. Along these lines, we saw a greater number of significant DEGs in WT compared to TAU when evaluating aging changes from 20-mo to 10-mo in almost all major cell types. In astrocytes, common genes that increased with age in both Tau and WT included *Cntnap2*, *A2m*, *Gfap*, and others. *A2m* has been shown to accumulate in fibroblasts with aging⁷⁵ and has been linked to tau phosphorylation and development of AD⁷⁶. Interestingly, *Fbln2* was one of the top upregulated genes in astrocytes in WT-20mo compared to Tau-20mo, but did not differ between Tau-20mo and WT-20mo. We suggest, in agreement with others, that tauopathy in AD accelerates the course of neurodegeneration during aging. Thus, we propose that the R955-hTau rat model is useful for investigating the compensatory events for synaptic dysfunction in the early phase of AD that are ultimately depleted when faced with insurmountable tauopathy. Our motif analysis based on differentially accessible peaks revealed transcription factors, such as *GSX2* in astrocytes, *MEF2D* in microglia, and *SOX15* in oligodendrocytes, suggesting the activation of stress-response pathways. For instance, *MEF2D* is a pro-survival factor upregulated after oxygen-glucose deprivation⁷⁷ and acts as an anti-inflammatory response to curb the expression of *NLRP3*, *IL-1 β* , and *iNOS*³³. At the same time, upregulation of TF, such as *DBP* in DG Glut in Tau at 10 months, may disrupt hippocampal neuronal function and enhance seizure susceptibility²⁷. Our spatial transcriptomics analysis found that *BDNF* signaling was reduced in the hippocampus in tau 10 and 20 months compared to WT. *BDNF* is a neurotrophic factor necessary for neurogenesis, regulating synaptic plasticity, and is depleted in neurodegenerative diseases, including AD⁷⁸. *BDNF* administration in the P301L transgenic mouse model of tauopathy reduced memory deficits, synaptic degeneration, and increased neurogenesis⁷⁹. However, therapeutic intervention using *BDNF* has proven challenging due to its short half-life, inability to cross the BBB⁸⁰, and side effects such as weight loss and anorexia⁸¹.

Our work from other labs has demonstrated that polyunsaturated fatty acids, such as DHA, and downstream lipid mediators, such as *NPD1*, may protect against dendritic spine loss and abnormal beading in an epileptic model⁸², and against LPS-induced dendritic spine abnormalities⁸³. More recently, we have demonstrated that lipid mediators derived from very-long-chain polyunsaturated fatty acids (VLC-PUFAs), such as elovanoids (ELVs)⁸⁴⁻⁸⁶, offer protection against neurodegenerative diseases, ischemic stroke, TBI, and amyloidopathy in the brain⁸⁷ and in the eye⁸⁸. As a future direction, we propose to test if ELVs may correct the synaptic dysfunction observed in early tauopathy, promoting the clearing of tau and reducing neuroinflammatory processes, thus allowing for the restoration of synaptic homeostasis.

Our results offered the first single-nuclei multiome examination of the R955-hTau rat model of tauopathy. However, there are several limitations to consider in the current study. We used a pseudo-bulked approach for differential expression and accessibility analysis, which aggregates cells to the sample level and performs differential testing using biological replicates. Thus, the low number of samples (three animals) per group limited the power analysis after adjustments for multiple testing. For spatial transcriptomics analysis, we used the mouse Visium probe set over rat tissue because the rat-specific probe set was unavailable. Yet, several previous studies have identified genes of interest using the Visium mouse probes on

rat tissue^{89,90}, likely due to the high degree of genomic homology between rat and mouse. Finally, our single-cell multiome study was limited to female animals. Many past studies have omitted the inclusion of female animals in AD research. We choose to focus on female rats due to the greater prevalence of AD occurring in females, as well as women experiencing higher rates of cognitive decline due to AD, and evidence of higher tau tangle density in women⁹¹.

Although we acknowledge the limitations of our study, the consistent changes observed for genes like *Chrm2* across various assays (snRNA, snATAC, spatial transcriptomics, and western blot) bolster our confidence in our findings and the identification of relevant pathways. Further investigations are necessary to dissect out the signaling mechanisms that alter synaptic changes found in neurons and glial cells. A review of NTN1 potential roles in AD highlights that diets poor in methionine and vitamins are associated with Netrin-1 hypermethylation and down expression and that NTN1 binding to UNC5C may inhibit neuronal cell death⁹². Mechanistic studies have found that NTN1/DCC activates PLC γ 1 Y783 phosphorylation, which turns on SRC Kinase and regulates actin rearrangement and axonal guidance⁹³. Moreover, NTN-1 has been shown to directly interact with tau protein⁷³ and interact with APP to suppress A β production⁷⁰. Future experiments, such as measuring NTN1 methylation changes in R955-hTau^{+/+} animals or overexpressing NTN1 in R955-hTau^{+/+} animals or in vitro models to measure neuron survival or neurite outgrowth after treatment with hTau P301S and/or NTN1, would provide insight into possible neuroprotective roles of NTN1 against AD tauopathy. Other assays that could provide functional validation of the shifts in glutamate receptor-mediated signaling include electrophysiology measurements of glutamate and GABAergic receptor activity in both Tau 10 and 20 months or calcium imaging. These assays would be invaluable to assess the strength of glutamatergic and GABAergic transmissions and synaptic plasticity that are crucial to memory function in the hippocampus that are compromised in early and late tauopathy. Further examination of microglia-synapse interactions would reveal mechanisms through which aberrant synaptic pruning may occur. While we have previously reported that *Iba1* expressing microglia are elevated at Tau 14 months, functional assessment of microglia derived from WT and Tau animals using engulfment assays of synaptosomes/fluorescent beads or high-resolution imaging of microglia-neuron co-cultures could be explored. Finally, ChIP-qPCR or ChIP-seq determination of MEF2 family of TF in microglia or ATF4 in neurons comparing Tau with WT at 10 and 20 months would better support our TF motif analysis.

In summary, this study identified specific markers and pathways of synaptic disruptions using a single-nuclei multiome and spatial transcriptomics approach that define new markers for tau-driven AD pathology and offered single-cell evidence of genes implicated in AD. These results reveal alterations in cell communication of glutamatergic transmission and Netrin signaling due to tauopathy that will be further explored. Finally, our data contributes to established synaptic dysfunctions as a hallmark of AD and offers targets for future mechanistic investigations and to develop therapeutic avenues for AD.

Methods

Animals

The McGill-R955-hTau transgenic rat was generated as previously detailed¹¹. These rats overexpress the coding region of the 2N4R isoform of human tau with the P301S missense mutation, which is linked to FTDP-17⁹⁴. The CaMKII- α promoter ensures expression is targeted to excitatory neurons in the forebrain, preventing overexpression in motor regions. The rats were housed in groups of 3–4 in a GR1800 double-decker cage system (Techniplast, Int.) under a 12:12 light: dark cycle, with standard chow and water available ad libitum. The study's use of animals was approved by the McGill Animal Care Committee, following the guidelines of the Canadian Council on Animal Care (CCAC). We have complied with all relevant ethical regulations for animal use. The sex, age, and genotype of animals are detailed in Supplementary Table 1.

Single-cell multiome

Hippocampus from 10-month and 20-month-old female McGill-R955-hTau transgenic rats and age-matching WT controls were dissected and snap-frozen at -80 °C until further use. The tissues were minced and homogenized, and single-nuclei were isolated following 10x Genomics protocol (Pleasanton, CA, CG000505). Briefly, frozen tissues were minced, lysed, and dissociated in lysis buffer and then filtered on Nuclei Isolation Column by centrifugation. Nuclei pellets were washed with debris removal buffer, and nuclei were resuspended with 50 μ L resuspension buffer. Nuclei concentration was determined with Luna-FL cell counter (Logos Biosystems, Annandale, VA). Using the 10x Genomics Chromium Controller and following downstream protocols, RNA and ATAC libraries were generated on a cell-by-cell basis using microfluidic partitioning to capture single cells and prepare barcoded, next-generation sequencing (NGS) libraries. The mRNA and ATAC libraries were sequenced using a NovaSeq 6000 system (Illumina, San Diego, CA), targeting at minimum 80,000 and 50,000 reads per cell for mRNA and ATAC, respectively.

Spatial transcriptomics

10-month and 20-month-old female McGill-R955-hTau transgenic rats and age-matching WT controls were perfused with 10% formalin, and the fixed brains were embedded in OCT compound, coronally sectioned at 10 μ m using CryoStar NX50 cryotome (Eppredia Kalamazoo, MI), and mounted onto microscope slides. Tissue sections were transferred onto the fiducial frames of a Visium Spatial Gene Expression slide (PN-2000233, 10x Genomics, Pleasanton, CA) using the Visium CytAssist. The tissues underwent spatial barcoding, and cDNA library was generated from the tissue mRNA as outlined in the Visium Spatial Gene Expression User Guide (CG000239, 10x Genomics). The mRNA transcriptome was mapped to a 55 μ m spatial resolution, corresponding to 1–10 cells per spot. The mRNA library was sequenced using a NextSeq 2000 platform.

Bioinformatic analysis of multiome

Data pre-processing and quality control. Filtered feature matrices and ATAC fragments for each sample were input and merged to create a Seurat Object in R. RNA filtering was performed by removing all cells with $200 < nFeature_RNA < 5000$ and cells with $> 15\%$ mitochondrial genes. ATAC filtering was performed by removing all cells with $TSS.enrichment < 2$ and cells with $nCount_ATAC < 1000$ or $> 100,000$. The distribution of RNA and ATAC quality control (QC) data before and after filtering is shown in Supplementary Figs. 27 and 28. DoubletFinder was performed with an expected rate of 7.5%, and multiples were filtered out. An example of doublet finder is shown in Supplementary Fig. 29. ATAC assay was annotated using mRatBN7.2. Peaks were called using MACS2⁹⁵ used in CallPeaks function in Signac. Signac was used to correlate peaks to the expression of nearby genes using the LinkPeaks function⁹⁶.

Normalization, clustering, and cell type annotation. SCTransform normalization and Principal Component Analysis (PCA) were performed on RNA. Dimensionality reduction was conducted using PCA dimensions 1:50 and a clustering resolution of 1.0 to create RNA UMAP. Frequency-inverse document frequency (TF-IDF) and SVD normalization were performed on ATAC assay for (latent semantic indexing; LSI) reduction. Dimensionality reduction was performed using LSI dimensions 2:25 and a clustering resolution of 1.0 to create ATAC UMAP. The standard deviation for the PCA and LSI components is presented as elbow plots in Supplementary Fig. 30. Both UMAPs were integrated using Weighted Nearest Neighbor (WNN) analysis. WNN dimensionality reduction was performed using PCA and LSI dimensions described above and a resolution of 2.0 for clustering. We then generated a multimodal UMAP based on performed weighted nearest neighbor clustering of paired snRNA and snATAC data, which demonstrated the separation of cells into trajectory-guided clusters (Fig. 1a). Unbiased analysis revealed 57 clusters. We mapped our RNA dataset to the Allen

Brain Cell (ABC) Atlas (RRID:SCR_024440) 10x Whole Mouse Brain taxonomy using the tool MapMyCells and the Hierarchical Mapping algorithm⁹⁷. Cluster labels from MapMyCells output were manually added to initial Seurat Clusters to maximize clarity and labels were confirmed with known cell markers and top markers from Seurat FindAllMarkers function between clusters (Fig. 1b).

Differential expression (DE) and differential accessibility (DA) Analysis. Differential gene expression analysis was conducted to determine the effect of tau mutation and the effects of aging in Tau and WT animals. We employed a pseudobulked approach to DE by averaging expression data at the sample level using the Seurat function AggregateExpression. Bulk data was normalized and scaled in Seurat. We pre-filtered for genes that were expressed in at least 5% of cells in at least one of the groups being compared. Comparisons were made at the sample level using DESeq2 function implemented in Seurat and Benjamini and Hochberg method for multiple test correction. DEGs for each cell type were visualized using EnhancedVolcano to observe log₂FoldChange and significance (-log₁₀P). Differential Accessibility was conducted similarly to DE, with the exception of the pre-filtering step, using sample level accessibility data processed through DESeq2. Additional annotation was generated for each peak using ClosestFeature function from Signac to identify nearby genes. Visualization was performed using CMplot to generate an epigenome-wide display of differentially accessible regions (DARs) between conditions.

In addition to pseudobulking approach, DE was performed using a mixed-effect model using Nebula⁹⁸ and using non-aggregated data in Seurat. A model matrix was constructed from the Seurat object using scToNeb function using normalized gene expression data and cells were grouped by individual sample. Nebula function was run for each cell type using the model matrix. Non-aggregated DE was performed between conditions for each cell type using Seurat FindMarkers function and the Wilcoxon Rank Sum Test. The data tables from the alternative statistical models can be found in Supplementary Dataset 2 and 3.

Gene ontology (GO) pathway analysis. Top differentially expressed gene (DEG) lists were generated from the DE analysis listed above by selecting the top 300 significant DEGs ranked by p-value for each comparison. The gene lists were implemented into clusterProfiler to determine the enrichment of GO classifications. Comparisons between Tau and WT at each age group, as well as between early and late age groups, were made for each cell type using the compareCluster function. Visualizations of top significant and relevant pathways for comparisons were plotted using DOSE and enrichR packages. Heatmaps for all the genes in the pathways shown for each cell type were generated using dittoHeatmap function from dittoSeq package.

Motif enrichment analysis. To compare differences in TF activity, we first used ChromVar to calculate z-scores for all motifs found in the JASPAR2020 vertebrate motif database for each⁹⁹. Next, the Seurat function FindMarkers was run between different conditions for each cell type on the Chromvar assay in Seurat using row means of motif accessibility to identify average difference. Top differentially accessible motifs for each comparison were shown in Doplots. Consensus sequences of motifs of interest were plotted using MotifPlot, and cell type-specific differences between conditions were visualized using RidgePlots.

Cell-cell communication analysis using CellChat. A subset for each condition in Seurat and CellChat¹⁰⁰ objects was created using the RNA assay. The CellChatDB.mouse annotation was applied, and subsetDB was run to include all but non-protein signaling from the CellChat database. For each CellChat object, identifyOverExpressedGenes and identifyOverExpressedInteractions were run to identify ligand-receptor pairs (LRPs) from each subset for further analysis. Cell-Cell

communication was determined by computeCommunProb using tri-Means, and communications were summarized by pathway and aggregated for each cell type using computeCommunProbPathway and aggregateNet. Inferred communications with less than 10 cells were filtered out. Systems analysis to map dominant senders, receivers, mediators, and influencers in computed communication was done using netAnalysis_computeCentrality, and signaling network similarity was determined using computeNetSimilarity. Comparative analysis between conditions was conducted by merging CellChat objects using merge-CellChat, and communication differences were determined between conditions using computeNetSimilarityPairwise. Differences in the number of interactions and interaction strength were visualized using compareInteractions for bar plots and netVisual_diffInteraction for circular plots. Differences in interactions between conditions by cell type were visualized by netAnalysis_diff_signaling_Role_scatter. Specific interaction pathways within cell types were observed using netAnalysis_signalingChanges_scatter. Visualization of changes in specific LRPs between cell types for Netrin signaling was generated using netVisual_bubble specifying Netrin signaling pathway. Change in information flow in Netrin pathway between comparisons was visualized using RankNet.

Cell-Cell communication analysis using NeuronChat. The same subset from Seurat listed above was used to generate NeuronChat¹⁴ objects for each condition using RNA assay. Each cell type was given an additional classification of Glutamatergic, GABAergic, or non-neuron based on Seurat annotation. NeuronChat communication analysis was performed for each object using run_NeuronChat with a permutation test set to M = 100. Communications were aggregated for each cell type using net_aggregation. NeuronChat objects were merged for comparative analysis using merge_NeuronChat. Differences in the number of interactions and interaction strength between conditions were visualized using compareInteractions_Neuron for bar plots and netVisual_circle_neuron for circle plots. Differences in signaling of specific LRPs between conditions were visualized using rankNet_Neuron.

Trajectory analysis. A Seurat object containing only DG Glut neurons and SCT normalized RNA data was created from the processed Multiome data. To cluster cells, principal components were generated using RunPCA, and the top 10 reduced dimensions were used for FindNeighbors and RunUMAP and a resolution of 1 for FindClusters. The Seurat object was converted to a Cell Data Set (CDS) object using Seurat Wrapper as.cell_data_set. The CDS object was processed using Monocle3 workflow, including preprocess_cds, reduce_dimensions, cluster_cells, learn_graph, and order_cells in sequence. The starting position for pseudotime calculation was chosen as the node with the highest distribution of cells from the WT_10mo samples. Pseudotime information was transferred back to the Seurat object using AddMetaData.

Bioinformatics analysis of spatial transcriptomics

Data processing. Outputs from sequencing and images were loaded into R as Seurat objects. Each object was normalized using SCTransform and then merged together. PCA was conducted, and dimensions 1:40 were used for UMAP generation with a clustering resolution of 0.5. Clusters were annotated based on gene markers as well as anatomical position.

Differential expression analysis and GO enrichment. Differential expression testing between conditions for each cell type was performed using FindMarkers in Seurat. GO enrichment was performed as described above in Multiome analysis.

Cell-cell communication analysis using CellChat. Seurat objects for each condition were used to create CellChat objects. Image information was gathered using GetTissueCoordinates in Seurat and scale factors

from sequencing were acquired from JSON files. Spatial factors for CellChat initiation were calculated by dividing the theoretical spot size of 65 μm by the acquired scale factors to create a conversion ratio. CellChat object processing was conducted as described above in Multiome analysis, except for using truncatedMeans instead of triMeans. Comparative analysis was performed by merging CellChat objects.

Molecular approaches

Capillary Western blot assay. Hippocampus from McGill-R955-hTau female transgenic rats (10-month) was homogenized and sonicated using RIPA buffer (ProteinSimple, San Jose, CA, #PN/ 040-483). Soluble protein concentration was determined by BCA assay (Thermo Fisher Scientific, Cat. 23225) and 0.4 μg used/reaction. Samples were heated at 95 $^{\circ}\text{C}/5$ min, and 3 μL of each sample were loaded. The 12–230 kDa cartridge (Protein Simple, #SM-W004) was used. Primary antibodies were diluted in antibody diluent 2 buffer (Protein Simple, #042-203), and the working solution of secondary antibodies was provided by the company (Protein Simple, #042-206). For data analysis, the area of spectra that matched the molecular weight of the target protein was used, and the normalization was performed using total protein stain. Primary antibodies are listed in Supplementary Table 2.

Immunohistochemistry and microscopy. For immuno-labeling, coronal brain sections from each animal (see details in *Spatial transcriptomics* section) were washed three times in 1X PBS for 5 min each, then permeabilized with 1X PBS containing 0.1% Triton X-100 (PBST). The tissues were blocked in PBST with 5% normal goat serum for 1.5 to 2 h at room temperature (RT). After blocking, the tissues were incubated overnight at 4 $^{\circ}\text{C}$ with primary antibodies (see Supplementary Table 2) diluted in 1% goat serum/PBST. The next day, the tissues were washed three times in PBST for 5 min each, then incubated with secondary antibodies diluted in 1% goat serum/PBST (1:500, Dylight-/Alexa-conjugated antibodies, Thermo Fisher Scientific, Whatman, MA) for 2 h at RT. For nuclear staining, Hoechst (1:10,000) was diluted in PBST and incubated with the tissues for 15 min, followed by three 10-min washes with PBST. Prolong Gold antifade reagent (Thermo Fisher Scientific) was used to mount the coverslips onto the slides. Brains were imaged using an FV3000 Olympus confocal microscope with a 40X long-range objective. Z-stacks with 1 μm step-size were acquired in four different areas of the brain for each antibody tested. Maximal projections of the z-stacks were captured and exported in Fiji¹⁰¹ for fluorescence intensity measurements.

Statistical analysis and reproducibility

For the analysis of multiome and spatial transcriptomic data, plots were generated in R using either the ggplot2 package or Seurat, with custom code modifications for data visualization. All p-values reported in this study were adjusted for false discovery rate (FDR) using the Benjamini–Hochberg procedure for differential expression (DE) analysis or the Bonferroni method for all other analyses. P-values below 0.05 were considered statistically significant. Three rats per group were chosen for the multiome analysis to enable pseudobulked analysis of the data.

Statistical analyses and figures of the protein quantification from capillary Western Blot were performed using GraphPad Prism version 10, using Student's *t* test. All group data are presented as mean \pm SEM. Significance was defined when $p < 0.05$.

Data availability

The datasets generated and analyzed during the current study are available from the corresponding author upon request. Additionally, the raw sequencing data have been deposited in Gene Expression Omnibus (GEO) under the accession GSE305314. All other relevant data supporting the findings of this study are included within the manuscript and its supplementary information files. Numerical source data underlying the graphs in the paper can be found in Supplementary Data File 6.

Code availability

All analysis was performed using publicly available tools and packages in R. Analytical workflow is outlined in the Methods section. Specific code is available upon reasonable request.

Received: 13 January 2025; Accepted: 26 September 2025;

Published online: 17 November 2025

References

- Liu, E., Zhang, Y. & Wang, J.-Z. Updates in Alzheimer's disease: from basic research to diagnosis and therapies. *Transl. Neurodegener.* **13**, 45 (2024).
- Abdul Manap, A. S. et al. Alzheimer's disease: a review on the current trends of the effective diagnosis and therapeutics. *Front. Aging Neurosci.* **16**, 1429211 (2024).
- Querfurth, H. W. & LaFerla, F. M. Alzheimer's disease. *N. Engl. J. Med.* **362**, 329–344 (2010).
- Götz, J., Bodea, L.-G. & Goedert, M. Rodent models for Alzheimer disease. *Nat. Rev. Neurosci.* **19**, 583–598 (2018).
- Götz, J. et al. Transgenic animal models of Alzheimer's disease and related disorders: histopathology, behavior and therapy. *Mol. Psychiatry* **9**, 664–683 (2004).
- Spires, T. L. & Hyman, B. T. Transgenic models of Alzheimer's disease: learning from animals. *NeuroRx* **2**, 423–437 (2005).
- Do Carmo, S. & Cuervo, A. C. Modeling Alzheimer's disease in transgenic rats. *Mol. Neurodegener.* **8**, 37 (2013).
- Hanes, J. et al. Rat tau proteome consists of six tau isoforms: implication for animal models of human tauopathies. *J. Neurochem.* **108**, 1167–1176 (2009).
- Hernández, F., Merchán-Rubira, J., Vallés-Saiz, L., Rodríguez-Matellán, A. & Avila, J. Differences between human and murine tau at the N-terminal end. *Front. Aging Neurosci.* **12**, 11 (2020).
- Habif, M. et al. Early long-term memory impairment and changes in the expression of synaptic plasticity-associated genes, in the McGill-R-Thy1-APP rat model of Alzheimer's-like brain amyloidosis. *Front. Aging Neurosci.* **12**, 585873 (2020).
- Emmerson, J. T. et al. Progressive human-like tauopathy with downstream neurodegeneration and neurovascular compromise in a transgenic rat model. *Neurobiol. Dis.* **184**, 106227 (2023).
- Santacruz, K. et al. Tau suppression in a neurodegenerative mouse model improves memory function. *Science* **309**, 476–481 (2005).
- Kamat, P. K. et al. Mechanism of oxidative stress and synapse dysfunction in the pathogenesis of Alzheimer's disease: understanding the therapeutics strategies. *Mol. Neurobiol.* **53**, 648–661 (2016).
- Zhao, W., Johnston, K. G., Ren, H., Xu, X. & Nie, Q. Inferring neuron-neuron communications from single-cell transcriptomics through NeuronChat. *bioRxiv* <https://doi.org/10.1101/2023.01.12.523826> (2023).
- Rombaut, B. et al. PDE inhibition in distinct cell types to reclaim the balance of synaptic plasticity. *Theranostics* **11**, 2080–2097 (2021).
- Heckman, P. R. A., Wouters, C. & Prickaerts, J. Phosphodiesterase inhibitors as a target for cognition enhancement in aging and Alzheimer's disease: a translational overview. *Curr. Pharm. Des.* **21**, 317–331 (2015).
- Mao, X., Gu, X. & Lu, W. GSG1L regulates the strength of AMPA receptor-mediated synaptic transmission but not AMPA receptor kinetics in hippocampal dentate granule neurons. *J. Neurophysiol.* **117**, 28–35 (2017).
- Lovero, K. L., Blankenship, S. M., Shi, Y. & Nicoll, R. A. SynDIG1 promotes excitatory synaptogenesis independent of AMPA receptor trafficking and biophysical regulation. *PLoS ONE* **8**, e66171 (2013).
- Zou, P., Wu, C., Liu, T. C.-Y., Duan, R. & Yang, L. Oligodendrocyte progenitor cells in Alzheimer's disease: from physiology to pathology. *Transl. Neurodegener.* **12**, 52 (2023).

20. Cai, M. et al. Insights from the neural guidance factor Netrin-1 into neurodegeneration and other diseases. *Front. Mol. Neurosci.* **17**, 1379726 (2024).
21. Wetzel-Smith, M. K. et al. A rare mutation in UNC5C predisposes to late-onset Alzheimer's disease and increases neuronal cell death. *Nat. Med.* **20**, 1452–1457 (2014).
22. López-Juárez, A. et al. Gsx2 controls region-specific activation of neural stem cells and injury-induced neurogenesis in the adult subventricular zone. *Genes Dev.* **27**, 1272–1287 (2013).
23. Lu, F. et al. Regulation of IFN-Is by MEF2D Promotes Inflammatory Homeostasis in Microglia. *J. Inflamm. Res.* **14**, 2851–2863 (2021).
24. Shi, L. et al. MEF2D participates in microglia-mediated neuroprotection in cerebral ischemia-reperfusion rats. *Shock* **57**, 118–130 (2022).
25. Choi, E.-B. et al. Transcription factor SOX15 regulates stem cell pluripotency and promotes neural fate during differentiation by activating the neurogenic gene Hes5. *J. Biol. Chem.* **299**, 102996 (2023).
26. Pecce, V. et al. The role of FOSL1 in stem-like cell reprogramming processes. *Sci. Rep.* **11**, 14677 (2021).
27. Klugmann, M. et al. A novel role of circadian transcription factor DBP in hippocampal plasticity. *Mol. Cell Neurosci.* **31**, 303–314 (2006).
28. Corona, C. et al. Activating transcription factor 4 (ATF4) regulates neuronal activity by controlling GABABR trafficking. *J. Neurosci.* **38**, 6102–6113 (2018).
29. Liu, J., Pasini, S., Shelanski, M. L. & Greene, L. A. Activating transcription factor 4 (ATF4) modulates post-synaptic development and dendritic spine morphology. *Front. Cell Neurosci.* **8**, 177 (2014).
30. Pasini, S., Corona, C., Liu, J., Greene, L. A. & Shelanski, M. L. Specific downregulation of hippocampal ATF4 reveals a necessary role in synaptic plasticity and memory. *Cell Rep.* **11**, 183–191 (2015).
31. Zhu, Q. et al. The transcription factor Pou3f1 promotes neural fate commitment via activation of neural lineage genes and inhibition of external signaling pathways. *Elife* **3**, e02224 (2014).
32. Liu, C. et al. GA-binding protein GABPβ1 is required for the proliferation of neural stem/progenitor cells. *Stem Cell Res.* **39**, 101501 (2019).
33. Hashizume, K., Yamanaka, M. & Ueda, S. POU3F2 participates in cognitive function and adult hippocampal neurogenesis via mammalian-characteristic amino acid repeats. *Genes Brain Behav.* **17**, 118–125 (2018).
34. Martins, S. A. et al. CD81 promotes a migratory phenotype in neuronal-like cells. *Microsc. Microanal.* **25**, 229–235 (2019).
35. Satoh, J.-I., Yamamoto, Y., Asahina, N., Kitano, S. & Kino, Y. RNA-Seq data mining: downregulation of NeuroD6 serves as a possible biomarker for Alzheimer's disease brains. *Dis. Markers* **2014**, 123165 (2014).
36. Miyashita, A. et al. Genes associated with the progression of neurofibrillary tangles in Alzheimer's disease. *Transl. Psychiatry* **4**, e396 (2014).
37. Wang, Z.-H. et al. Deficiency in BDNF/TrkB neurotrophic activity stimulates δ-secretase by upregulating C/EBPβ in Alzheimer's disease. *Cell Rep.* **28**, 655–669.e5 (2019).
38. Tzioras, M., McGeachan, R. I., Durrant, C. S. & Spires-Jones, T. L. Synaptic degeneration in Alzheimer disease. *Nat. Rev. Neurol.* **19**, 19–38 (2023).
39. Ali, M. et al. Single cell transcriptome analysis of the THY-Tau22 mouse model of Alzheimer's disease reveals sex-dependent dysregulations. *Cell Death Discov.* **10**, 119 (2024).
40. Woo, M. S. et al. Neuronal metabotropic glutamate receptor 8 protects against neurodegeneration in CNS inflammation. *J. Exp. Med.* **218**, e20201290 (2021).
41. Crimins, J. L., Rocher, A. B. & Luebke, J. I. Electrophysiological changes precede morphological changes to frontal cortical pyramidal neurons in the rTg4510 mouse model of progressive tauopathy. *Acta Neuropathol.* **124**, 777–795 (2012).
42. Crimins, J. L. et al. Homeostatic responses by surviving cortical pyramidal cells in neurodegenerative tauopathy. *Acta Neuropathol.* **122**, 551–564 (2011).
43. Emmerson, J. T. et al. Paradoxical attenuation of early amyloid-induced cognitive impairment and synaptic plasticity in an aged APP/Tau bigenic rat model. *Acta Neuropathol. Commun.* **12**, 193 (2024).
44. Monaco, M., Trebesova, H. & Grilli, M. Muscarinic receptors and Alzheimer's disease: new perspectives and mechanisms. *Curr. Issues Mol. Biol.* **46**, 6820–6835 (2024).
45. Lachowicz, J. E. et al. Facilitation of acetylcholine release and improvement in cognition by a selective M2 muscarinic antagonist, SCH 72788. *Life Sci.* **68**, 2585–2592 (2001).
46. Lai, M. K. et al. Psychosis of Alzheimer's disease is associated with elevated muscarinic M2 binding in the cortex. *Neurology* **57**, 805–811 (2001).
47. Gosso, F. M. et al. Exploring the functional role of the CHRM2 gene in human cognition: results from a dense genotyping and brain expression study. *BMC Med Genet.* **8**, 66 (2007).
48. McKenna, A. et al. KarXT for schizophrenia-effectiveness and value: a summary from the Institute for Clinical and Economic Review's New England Comparative Effectiveness Public Advisory Council. *J. Manag. Care Spec. Pharm.* **30**, 624–628 (2024).
49. Krystal, J. H. et al. Emraclidine, a novel positive allosteric modulator of cholinergic M4 receptors, for the treatment of schizophrenia: a two-part, randomised, double-blind, placebo-controlled, phase 1b trial. *Lancet* **400**, 2210–2220 (2022).
50. Tobin, A. B. A golden age of muscarinic acetylcholine receptor modulation in neurological diseases. *Nat. Rev. Drug Discov.* **23**, 743–758 (2024).
51. Fasciani, I. et al. The C-terminus of the prototypical M2 muscarinic receptor localizes to the mitochondria and regulates cell respiration under stress conditions. *PLoS Biol.* **22**, e3002582 (2024).
52. Bartolome, F., Carro, E. & Alquezar, C. Oxidative stress in tauopathies: from cause to therapy. *Antioxidants (Basel)* **11**, 1421 (2022).
53. Vrillon, A. et al. Plasma neuregulin 1 as a synaptic biomarker in Alzheimer's disease: a discovery cohort study. *Alzheimers Res. Ther.* **14**, 71 (2022).
54. Oichi, T. et al. Adamts17 is involved in skeletogenesis through modulation of BMP-Smad1/5/8 pathway. *Cell Mol. Life Sci.* **76**, 4795–4809 (2019).
55. Sidoryk-Węgrzynowicz, M., Adamiak, K. & Strużyńska, L. Astrocyte-neuron interaction via the glutamate-glutamine cycle and its dysfunction in tau-dependent neurodegeneration. *Int J. Mol. Sci.* **25**, 3050 (2024).
56. Javanmehr, N., Saleki, K., Alijanizadeh, P. & Rezaei, N. Microglia dynamics in aging-related neurobehavioral and neuroinflammatory diseases. *J. Neuroinflammation* **19**, 273 (2022).
57. Kuhn, S., Gritti, L., Crooks, D. & Dombrowski, Y. Oligodendrocytes in development, myelin generation and beyond. *Cells* **8**, 1424 (2019).
58. Hill, R. A., Nishiyama, A. & Hughes, E. G. Features, fates, and functions of oligodendrocyte precursor cells. *Cold Spring Harb. Perspect. Biol.* **16**, a041425 (2024).
59. Ghorbani, S. et al. Fibulin-2 is an extracellular matrix inhibitor of oligodendrocytes relevant to multiple sclerosis. *J. Clin. Invest.* e176910 (2024) <https://doi.org/10.1172/JCI176910> (2024).
60. Shultz, S. R. et al. Temporal proteomics of human cerebrospinal fluid after severe traumatic brain injury. *J. Neuroinflammation* **19**, 291 (2022).
61. Bader, J. M. et al. Proteome profiling in cerebrospinal fluid reveals novel biomarkers of Alzheimer's disease. *Mol. Syst. Biol.* **16**, e9356 (2020).

62. Patel, M. R. & Weaver, A. M. Astrocyte-derived small extracellular vesicles promote synapse formation via fibulin-2-mediated TGF- β signaling. *Cell Rep.* **34**, 108829 (2021).
63. Chen, B. et al. Proteomics of serum exosomes identified fibulin-1 as a novel biomarker for mild cognitive impairment. *Neural Regen. Res.* **18**, 587–593 (2023).
64. Serafini, T. et al. The netrins define a family of axon outgrowth-promoting proteins homologous to *C. elegans* UNC-6. *Cell* **78**, 409–424 (1994).
65. Kennedy, T. E., Serafini, T., de la Torre, J. R. & Tessier-Lavigne, M. Netrins are diffusible chemotropic factors for commissural axons in the embryonic spinal cord. *Cell* **78**, 425–435 (1994).
66. Goldman, J. S. et al. Netrin-1 promotes excitatory synaptogenesis between cortical neurons by initiating synapse assembly. *J. Neurosci.* **33**, 17278–17289 (2013).
67. Glasgow, S. D. et al. Activity-dependent Netrin-1 secretion drives synaptic insertion of GluA1-containing AMPA receptors in the hippocampus. *Cell Rep.* **25**, 168–182.e6 (2018).
68. Glasgow, S. D. et al. Pre- and post-synaptic roles for DCC in memory consolidation in the adult mouse hippocampus. *Mol. Brain* **13**, 56 (2020).
69. Shabani, M. et al. Netrin-1 improves the amyloid- β -mediated suppression of memory and synaptic plasticity. *Brain Res. Bull.* **131**, 107–116 (2017).
70. Lourenço, F. C. et al. Netrin-1 interacts with amyloid precursor protein and regulates amyloid-beta production. *Cell Death Differ.* **16**, 655–663 (2009).
71. Ju, T. et al. Decreased Netrin-1 in mild cognitive impairment and alzheimer's disease patients. *Front. Aging Neurosci.* **13**, 762649 (2021).
72. Sun, L. et al. Decreased Netrin-1 and correlated Th17/Tregs balance disorder in A β 1-42 induced Alzheimer's disease model rats. *Front Aging Neurosci.* **11**, 124 (2019).
73. Huang, H. et al. The role of microtubule-associated protein tau in netrin-1 attractive signaling. *J. Cell Sci.* **137**, jcs261244 (2024).
74. Wu, T. et al. Tau polarizes an aging transcriptional signature to excitatory neurons and glia. *Elife* **12**, e85251 (2023).
75. Kondo, T., Sakaguchi, M. & Namba, M. Two-dimensional gel electrophoretic studies on the cellular aging: accumulation of alpha-2-macroglobulin in human fibroblasts with aging. *Exp. Gerontol.* **36**, 487–495 (2001).
76. Varma, V. R. et al. Alpha-2 macroglobulin in Alzheimer's disease: a marker of neuronal injury through the RCAN1 pathway. *Mol. Psychiatry* **22**, 13–23 (2017).
77. Wang, N., Yang, W., Li, L. & Tian, M. MEF2D upregulation protects neurons from oxygen-glucose deprivation/re-oxygenation-induced injury by enhancing Nrf2 activation. *Brain Res.* **1741**, 146878 (2020).
78. Bathina, S. & Das, U. N. Brain-derived neurotrophic factor and its clinical implications. *Arch. Med Sci.* **11**, 1164–1178 (2015).
79. Jiao, S.-S. et al. Brain-derived neurotrophic factor protects against tau-related neurodegeneration of Alzheimer's disease. *Transl. Psychiatry* **6**, e907 (2016).
80. Poduslo, J. F. & Curran, G. L. Permeability at the blood-brain and blood-nerve barriers of the neurotrophic factors: NGF, CNTF, NT-3, BDNF. *Brain Res Mol. Brain Res.* **36**, 280–286 (1996).
81. Bartus, R. T. & Johnson, E. M. Clinical tests of neurotrophic factors for human neurodegenerative diseases, part 1: Where have we been and what have we learned? *Neurobiol. Dis.* **97**, 156–168 (2017).
82. Musto, A. E., Walker, C. P., Petasis, N. A. & Bazan, N. G. Hippocampal neuro-networks and dendritic spine perturbations in epileptogenesis are attenuated by neuroprotectin d1. *PLoS ONE* **10**, e0116543 (2015).
83. Chang, P. K.-Y., Khatchadourian, A., McKinney, R. A. & Maysinger, D. Docosahexaenoic acid (DHA): a modulator of microglia activity and dendritic spine morphology. *J. Neuroinflammation* **12**, 34 (2015).
84. Bazan, N. G. Docosanoids and elovanoids from omega-3 fatty acids are pro-homeostatic modulators of inflammatory responses, cell damage and neuroprotection. *Mol. Asp. Med.* **64**, 18–33 (2018).
85. Bhattacharjee, S. et al. Elovonoids are a novel class of homeostatic lipid mediators that protect neural cell integrity upon injury. *Sci. Adv.* **3**, e1700735 (2017).
86. Jun, B. et al. Elovonoids are novel cell-specific lipid mediators necessary for neuroprotective signaling for photoreceptor cell integrity. *Sci. Rep.* **7**, 5279 (2017).
87. Emre, C. et al. Age-related changes in brain phospholipids and bioactive lipids in the APP knock-in mouse model of Alzheimer's disease. *Acta Neuropathol. Commun.* **9**, 116 (2021).
88. Do, K. V. et al. Elovonoids counteract oligomeric β -amyloid-induced gene expression and protect photoreceptors. *Proc. Natl Acad. Sci. USA* **116**, 24317–24325 (2019).
89. Wang, C.-Y. et al. Rack1-mediated ferroptosis affects hindgut development in rats with anorectal malformations: Spatial transcriptome insights. *Cell Prolif.* **57**, e13618 (2024).
90. Wei, W. et al. In situ tissue profile of rat trigeminal nerve in trigeminal neuralgia using spatial transcriptome sequencing. *Int. J. Surg.* **110**, 1463–1474 (2024).
91. Oveisgharan, S. et al. Sex differences in Alzheimer's disease and common neuropathologies of aging. *Acta Neuropathol.* **136**, 887–900 (2018).
92. Zhang, L. et al. Roles and Mechanisms of Axon-Guidance Molecules in Alzheimer's Disease. *Mol. Neurobiol.* **58**, 3290–3307 (2021).
93. Kang, D.-S. et al. Netrin-1/DCC-mediated PLC γ 1 activation is required for axon guidance and brain structure development. *EMBO Rep.* **19**, e46250 (2018).
94. Bugiani, O. et al. Frontotemporal dementia and corticobasal degeneration in a family with a P301S mutation in tau. *J. Neuropathol. Exp. Neurol.* **58**, 667–677 (1999).
95. Zhang, Y. et al. Model-based analysis of ChIP-Seq (MACS). *Genome Biol.* **9**, R137 (2008).
96. Ma, S. et al. Chromatin potential identified by shared single-cell profiling of RNA and chromatin. *Cell* **183**, 1103–1116.e20 (2020).
97. Yao, Z. et al. A high-resolution transcriptomic and spatial atlas of cell types in the whole mouse brain. *Nature* **624**, 317–332 (2023).
98. He, L. et al. NEBULA is a fast negative binomial mixed model for differential or co-expression analysis of large-scale multi-subject single-cell data. *Commun. Biol.* **4**, 629 (2021).
99. Castro-Mondragon, J. A. et al. JASPAR 2022: the 9th release of the open-access database of transcription factor binding profiles. *Nucleic Acids Res.* **50**, D165–D173 (2022).
100. Jin, S. et al. Inference and analysis of cell-cell communication using CellChat. *Nat. Commun.* **12**, 1088 (2021).
101. Schindelin, J. et al. Fiji: an open-source platform for biological-image analysis. *Nat. Methods* **9**, 676–682 (2012).

Acknowledgements

This work was supported by the Eye, Ear, Nose & Throat (EENT) Foundation of New Orleans and the Bollinger Professorship. We are grateful to Dr. Jovanny Zabaleta and Dr. Jone Garai at the Translational Genomics Core Laboratory at the Stanley S. Scott Cancer Center, Louisiana State University Health Sciences Center, for their assistance with the QC on the multiome and QC and sequencing for the 10x Visium dataset. In addition, we would like to thank Camille Cannon and Paula Polk at the Genomics Core at LSU Health Shreveport for their assistance in the preparation and sequencing of the multiome libraries.

Author contributions

N.G.B. conceived and led the study. S.B. and J.X.J. generated single-cell and spatial sequencing libraries with assistance from A.P.M. J.X.J. and

B.L.G. led data analysis with assistance from S.B., M-A.I.K., and A.P.M. M-A.I.K performed immunohistochemistry and microscopy. S.D.C. and A.C.C. developed the model, provided brain samples, and participated in discussing conceptual aspects. S.B., J.X.J., B.L.G., M-A.I.K., and N.G.B. wrote the manuscript with input from all authors.

Competing interests

The authors declare no competing interests.

Additional information

Supplementary information The online version contains supplementary material available at <https://doi.org/10.1038/s42003-025-08959-z>.

Correspondence and requests for materials should be addressed to Nicolas G. Bazan.

Peer review information *Communications Biology* thanks Neelakshi Soni and the other, anonymous, reviewer(s) for their contribution to the peer review of this work. Primary Handling Editors: Joao Valente.

Reprints and permissions information is available at <http://www.nature.com/reprints>

Publisher's note Springer Nature remains neutral with regard to jurisdictional claims in published maps and institutional affiliations.

Open Access This article is licensed under a Creative Commons Attribution-NonCommercial-NoDerivatives 4.0 International License, which permits any non-commercial use, sharing, distribution and reproduction in any medium or format, as long as you give appropriate credit to the original author(s) and the source, provide a link to the Creative Commons licence, and indicate if you modified the licensed material. You do not have permission under this licence to share adapted material derived from this article or parts of it. The images or other third party material in this article are included in the article's Creative Commons licence, unless indicated otherwise in a credit line to the material. If material is not included in the article's Creative Commons licence and your intended use is not permitted by statutory regulation or exceeds the permitted use, you will need to obtain permission directly from the copyright holder. To view a copy of this licence, visit <http://creativecommons.org/licenses/by-nc-nd/4.0/>.

© The Author(s) 2025